Expert Systems With Applications 314 (2026) 131656

Contents lists available at ScienceDirect

Expert Systems With Applications

journal homepage: www.elsevier.com/locate/eswa

Fault-tolerant collaboration: A hierarchical control framework for traffic-communication systems at intersections with human-machine hybrid driving

Zhigang Wu [a,b], Haipeng Zeng [a,b], Di Wen [a,b,c], Huanting Xu [a,b], Zhaocheng He [a,b,c,*]

[a] School of Intelligent Systems Engineering, Sun Yat-sen University, Shenzhen Guangdong, China
[b] Guangdong Provincial Key Laboratory of Intelligent Transportation Systems, Shenzhen Guangdong, China
[c] Pengcheng Laboratory, Shenzhen Guangdong, China

ARTICLE INFO

Keywords:
Cyber-physical systems
Connected and autonomous vehicle
Human-machine hybrid driving
Vehicle-road collaboration
Internet of vehicles

ABSTRACT

At unsignalized intersections with human-machine mixed driving, a key challenge is enhancing the robustness of right-of-way (ROW) assignment while mitigating the cascading effects of uncertain behaviors from human drivers. This study introduces a fault-tolerant collaboration (FTC) strategy to address the problem. The key idea is to establish a hierarchical control framework to achieve cross-system optimization of traffic and communication for improving the efficiency of mixed traffic (including connected and autonomous vehicles and connected human-driven vehicles). Our method involves a tri-level model and a re-computation checker. In the upper level, we propose two collaboration mechanisms for ROW allocation scheme, aiming to minimize the likelihood of uncertain behaviors. The pessimistic estimation-based beam search is leveraged to expand the solution space. Then, the middle level builds the motif-based networking method, which contributes to generate scalable and reliable communication network. Based on the ROW allocation and communication networking scheme, vehicles exchanges information with effective filtered neighbors for local trajectory planning. We design a spatio-temporal embedded safety gap model in the lower level for local decision-making, addressing situations where there are unfeasible trajectory planning solutions due to uncertain behaviors. Finally, a re-computation checker is integrated to enhance the resilience of the strategy. The performance of the proposed method is evaluated through simulation experiments considering varying market penetration and vehicle violation rates. The results demonstrate that the FTC effectively mitigates the impact of uncertain behaviors, improving the strategy robustness and traffic efficiency, while maintaining low communication overhead and computational cost. Furthermore, the applicability of the proposed framework is validated through its transfer and evaluation at two real-world intersections, confirming its effectiveness and scalability under practical traffic conditions.

1. Introduction

With the continuous development of vehicle-to-everything (V2X) and artificial intelligence, autonomous driving has garnered significant attention (Feng et al., 2023; Preeti & Rana, 2024; Wang et al., 2024b; Zhang et al., 2025). However, achieving a fully autonomous driving environment requires extensive demonstration and practical application. During this transition, a mixed traffic system–where human-driven vehicles share the road with connected and automated vehicles (CAVs)–is an unavoidable intermediate stage (Chen et al., 2025; Li et al., 2024c; Sheng et al., 2024). Compared to traditional traffic systems, mixed traffic systems offer notable improvements in traffic efficiency (Amirgholy & Nourinejad, 2024), safety (Garg & Bouroche, 2023) and energy consumption (Greenblatt & Saxena, 2015), thereby promoting the sustainable development of urban environments and societies.

Intersections are among the primary bottlenecks in urban traffic networks and remain a significant challenge in the mixed traffic system (Chen et al., 2025; Jing et al., 2024). The high frequency of right-of-way (ROW) conflicts at intersections exacerbates the risk of traffic accidents. Unlike signalized intersections where signal control can be used to assign ROW (Guo & Ban, 2024; Wang et al., 2024a,c), it is significantly more difficult to resolve spatio-temporal conflicts at highly complex unsignalized intersections (Jing et al., 2024; Zhou et al., 2024). Addressing this issue requires the effective collaboration mechanism for

* Corresponding author.
E-mail addresses: wuzhg6@mail2.sysu.edu.cn (Z. Wu), zenghp5@mail.sysu.edu.cn (H. Zeng), wend25@mail2.sysu.edu.cn (D. Wen), xuht3@mail2.sysu.edu.cn (H. Xu), hezhch@mail.sysu.edu.cn (Z. He).

https://doi.org/10.1016/j.eswa.2026.131656
Received 5 May 2025; Received in revised form 9 September 2025; Accepted 10 February 2026
Available online 17 February 2026

human-machine mixed driving (HMMD), enabling ROW allocation to be negotiated through vehicle interactions.

In recent years, researchers have proposed various strategies based on individual interactions to address the ROW allocation problem in HMMD intersections (Shu et al., 2023; Zhang et al., 2023). Game theory has emerged as a promising method due to its ability to comprehensively analyze the dynamic dependencies within interaction processes (Qin et al., 2024). For instance, Li et al. (2024a) proposed a game-theoretic framework that integrates expert knowledge to manage intersection conflicts, thereby reducing the complexity of human-machine interaction. Similarly, Jia et al. (2023) developed a dynamic switching mechanism to decouple complex interactions, enabling vehicles to join or exit the game in real time and aligning decision-making more closely with human driving characteristics. Some studies have utilized naturalistic driving data to design payoff functions, in order to improve the understanding of human driving intentions and styles (Fang et al., 2024; Jing et al., 2024; Liu et al., 2024b). For example, Fang et al. (2024) applied inverse reinforcement learning to extract payoff preference features from the driving data, supporting the creation of a heterogeneous cooperative game framework. In an effort to enhance the social interaction capabilities of CAVs, Liu et al. (2024b) introduced a mixed-strategy game model to dynamically recognize driving styles, achieving effective conflict resolution and improved traffic efficiency. To further capture the coupling between vehicle interactions, some studies have combined traffic expertise with reinforcement learning, incorporating attention mechanisms to improve the accuracy of interaction modeling (Liu et al., 2024a,c; Sheng et al., 2024). Despite these advances, game-theoretic methodes still face some challenges. CAVs primarily adopt a passive role, focusing on understanding and responding to human driving behavior. Meanwhile, human decision-making remains heavily reliant on individual driving experience and judgment. This makes it difficult to actively guide or influence human driving behavior from the perspective of system-wide cooperative optimization.

Benefiting from connected technologies, swarm collaboration attempts to intervene in the behavior of connected human-driven vehicles (CHVs) to improve the safety and efficiency of human-machine hybrid driving (Liu et al., 2025). Some studies have explored human-machine interfaces (HMI) based on digital twins, offering cooperative guidance to CHVs while considering interactions with surrounding vehicles (Irfan et al., 2024; Li et al., 2024b). These guidance commands often generated from simple rules like first-in-first-out (FIFO), which tend to result in low traffic efficiency (Wang et al., 2022). To address this limitation, some researchers have proposed virtual formation-based reservation prioritization strategy (Chen et al., 2021). By leveraging graph-based conflict decomposition, these methods assign the same priority to conflict-free vehicles (Chen et al., 2022; Lin et al., 2019; Xu et al., 2018). Wu et al. (2024a) extends this concept with a "1 + n" mixed platoon control strategy. However, this approach requires that the platoon be formed upstream, which places strict requirements on the upstream platoon task. CHVs are not allowed to act as leaders, which ignores the uncertain behavior of CHVs when driving freely. Furthermore, Zhong et al. (2024) proposed a dynamic prioritization reservation strategy for traffic flow. Their method introduced an adaptive CAV re-planning mechanism for situations where CHVs do not participate in platoons. However, this approach adapts passively to the uncertain behavior of CHVs, which may lead to frequent re-reservations and thus increase computational costs. In addition, Zhou et al. (2024) developed a reinforcement learning framework based on an reasoning graph integrated with social rules. However, it does not consider the consequences of uncertain behavior, such as CHVs violating the rules. In summary, swarm collaboration still faces the challenge that uncertain human driving behavior may disrupt ROW allocation schemes. Therefore, a robust swarm collaboration strategy is desirable for ROW allocation.

The execution of the ROW allocation scheme in physical space depends on a reliable communication network that enables real-time information exchange between vehicles and the external environment. The tight coupling between traffic and communication systems is a key characteristic of cyber-physical systems (CPS) (Lin & Wei, 2023; Liu et al., 2022b; Sun et al., 2024; Zhao et al., 2023). However, unsignalized intersections face challenges such as non-line-of-sight (NLOS) occlusion and rapid vehicle movement, creating complex environments that exacerbate signal fading (Fang et al., 2022). Consequently, establishing a high-quality and stable communication topology for CPS in these settings is difficult. Some studies have adopted fixed-mode communication topologies for swarm collaboration in traffic scenarios (Wang et al., 2025), such as predecessor-leader following topology (PLF) (Chen et al., 2022) and multi-leader topology (MLT) (Chen et al., 2021). While these topologies are simple and can be quickly implemented, they fail to account for the complexity of the built environment and the motion dynamics of traffic flow (Long et al., 2022). To address this issue, previous studies have developed centralized periodic intervention communication networking methods (Wu et al., 2024b,c). They require precise vehicle location information to optimize the static topology over the intervention period. However, the optimized network topology lacks flexibility when the ROW allocation changes. Therefore, scalable communication networking methods are needed to adapt to the uncertainties inherent in the unsignalized intersection with HMMD.

To fill the gaps, this study proposes a fault-tolerant collaboration (FTC) strategy with hierarchical control. A cyber-physical system is developed for HMMD at the unsignalized intersection, utilizing an edge-end cooperative computing architecture. The ROW allocation and communication networking are implemented at the edge, optimizing the system from a global perspective. Each vehicle plans its trajectory based on edge-generated commands, enabling distributed decision-making at the individual level. Additionally, a re-computation checker at the edge is implemented to enhance the strategy resilience. The key contributions of this study are summarized as follows:

1) A collaboration mechanism incorporating exposure mitigation and risk retrospection is proposed to minimize the occurrence of uncertain behaviors for CHVs. A pessimistic estimation-based beam search algorithm is employed to optimize the efficiency of the ROW allocation scheme.
2) A motif-based dynamic-static coupling networking method is established to self-organize the generation of high-quality communication routing paths tailored to the intersection environment, while filtering effective interaction objects to reduce transmission and computational cost.
3) A spatio-temporal embedded safety gap model is designed to address situations where trajectory planning becomes infeasible due to the events triggered by unavoidable uncertain behaviors of CHVs, thus enhancing the fault tolerance of trajectory planning.

The remainder of this paper is organized as follows. Section 2 describes the problem and the cyber-physical system. Section 3 introduces the details of the proposed fault-tolerant collaboration strategy. In Section 4 we validate our method through a typical case and several simulation experiments with multiple scenarios. Section 5 summarizes some conclusions and suggestions.

2. Problem description

Fig. 1 illustrates the potential interactions within a typical CPS designed for an unsignalized intersection. The intersection features 4 arms, each comprising three lanes: a left-turn-only lane, a straight-only lane, and a mixed right-turn and straight-on lane. It is equipped with a roadside unit (RSU) and a mobile edge computing (MEC) server, which are interconnected via fiber optics. The intersection's control zone is defined based on the RSU's communication radius. All vehicles are assumed to be connected and equipped with on-board computing units (OBCUs), comprising both CAVs and CHVs. CAVs are assumed to make decisions and execute actions autonomously via their OBCUs. For CHVs, however, the OBCUs assist drivers by providing feedback through the HMI,

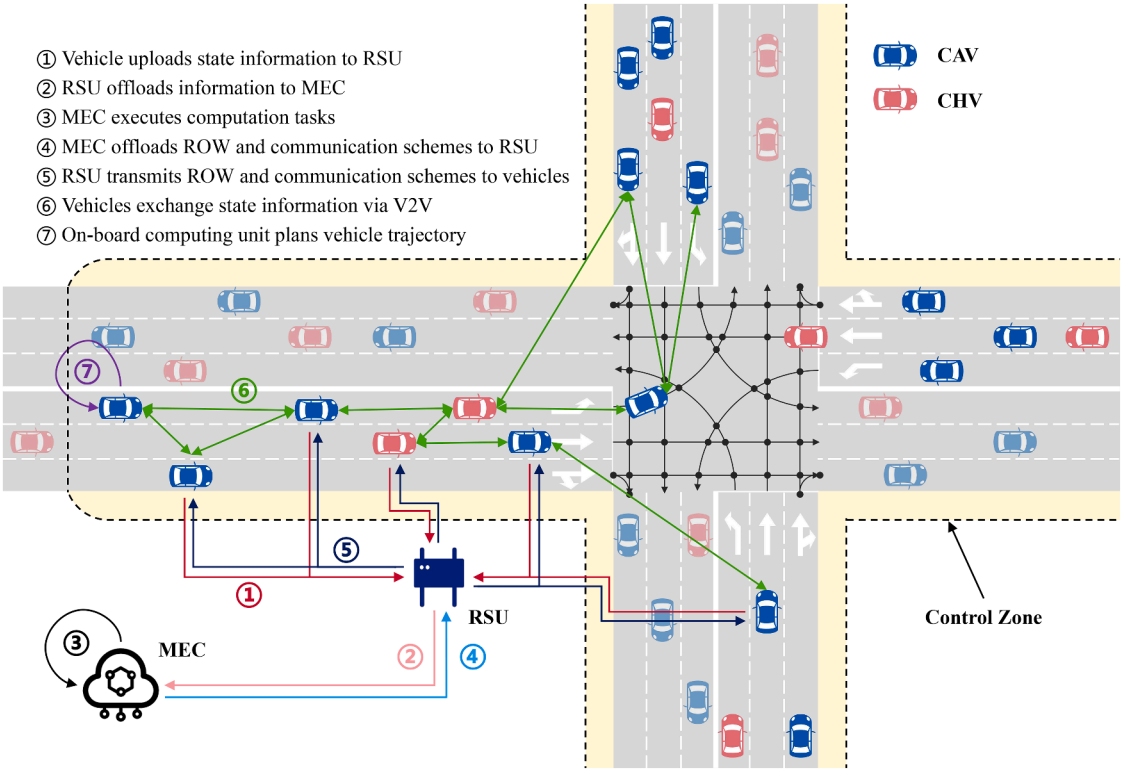

Fig. 1. A cyber-physical system for the unsignalized intersection with edge-end cooperative computation in 7 steps.

offering strategic recommendations and decision-making alerts to guide vehicle control (Wang et al., 2022).

Our main goal is to develop an effective ROW assignment and execution method. It will be achieved through edge-end cooperative computation. The problem-solving procedure is outlined in the seven steps depicted in Fig. 1. First, the RSU gathers state information from vehicles within the control zone (step 1) and offloads it to the MEC (step 2). Acting as a centralized decision-maker with a global perspective, the MEC develops optimal solutions for the transportation and communication systems (step 3). This involves solving a combinatorial optimization problem for ROW allocation to mitigate the impact of CHVs prioritizing individual benefits over system-wide efficiency. The resulting ROW scheme is encoded into commands and transmitted to vehicles via the RSU (steps 4 and 5). Once informed of the system's directives, vehicles engage in real-time interactions with their neighbors (step 6). Finally, the OBCUs independently generate fault-tolerant trajectory planning models to address potential CHV uncertain behaviors and minimize travel delays (step 7). Here we define uncertain behavior and establish two relevant assumptions.

Definition 1 (Uncertain Behaviors)**.** It is specifically defined as CHVs encroaching upon the ROW in violation of the assigned scheme, that is, occupying the ROW at their own discretion rather than queuing and yielding to conflicting vehicles as required.

Assumption 1. *When complying with commands, CHVs are assumed to trust the guidance and endeavor to follow the instructed trajectories. Once a violation intention arises, however, the CHV reverts to decision-making based on its individual driving model.*

Assumption 2. *Human drivers are generally inclined to pass through the intersection as quickly as possible under safety constraints. If a driver observes that a conflicting vehicle decelerates or even stops to yield, the driver is likely to proceed without hesitation (Fang et al., 2024; Zhong et al., 2024; Zhou et al., 2024).*

3. Hierarchical control method

3.1. Framework

The proposed hierarchical control method is composed of a tri-level structure along with a re-computation checker, as illustrated in Fig. 2:

1) Upper Level: The MEC develops an efficient and robust ROW allocation scheme for vehicle clusters. By searching for cliques on a heterogeneous graph, it ensures that no collisions occur between vehicles sharing the same ROW. Two collaborative mechanisms–exposure mitigation and risk retrospection–are introduced to reduce the likelihood of CHVs violating commands. This level primarily focuses on planning conflict-free reservation sequences from the perspective of road infrastructure.
2) Middle Level: Based on the ROW allocation constraints provided by the upper level, vehicles are filtered to identify effective interactions. A dynamic-static coupling network is then generated using motifs to meet the reliability requirements of frequent information exchanges. Through the communication network, vehicles share information with their effective neighbors.
3) Lower Level: Each vehicle formulates and solves a local safety gap model using its on-board computing unit. A rolling horizon-based distributed model predictive control (DMPC) is employed to plan the future trajectory for each vehicle. Vehicles execute the optimal actions, repeating the process until the entire vehicle cluster passes through the intersection. Note that we guide CHVs through the intersection by planning trajectories for interaction via EHMI. If drivers reject the assisted strategy, they rely on their own driving experience.

Additionally, a re-computation checker is designed to handle CHV command violations that disrupt the assigned ROW scheme. This module reassigns the ROW for vehicles that have not yet cleared the intersection. The hierarchical control strategy is then reactivated to update the allocation scheme, restoring the orderly operation of the intersection.

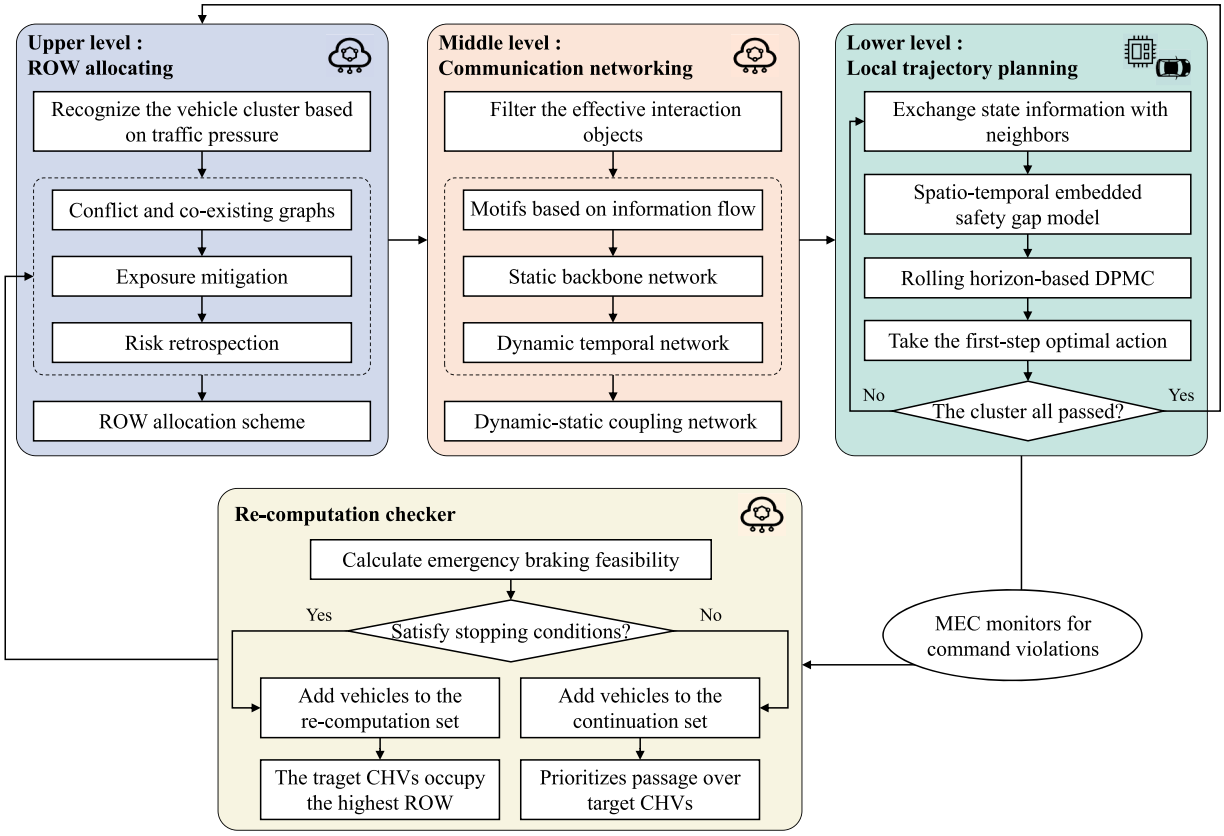

Fig. 2. The framework of the proposed fault-tolerant collaboration, including a tri-level structure along with a re-computation checker.

3.2. Upper level: ROW allocating

3.2.1. Classification of vehicle cluster

Due to variations in vehicle arrival rates from different directions, the number of vehicles waiting in each lane also differs. To ensure service equity, the size of the vehicle cluster served in each round will be allocated to each lane proportionally based on the queue length:

$$N_l^* = |\mathbb{V}_l| \frac{N_G}{N_{CZ}}, \forall l \in L \tag{1}$$

where N_l^* is the quota of lane l. $|\mathbb{V}_l|$ is the queue length of lane l. N_G and N_{CZ} are the cluster size and the number of all vehicles in the control zone, respectively. L is the set of lanes at the intersection. Subsequently, vehicles i in lane l will be added to the cluster $\mathbb{V}_l^*$ based on the distance $d_{i,l}$ from the vehicle i to the stop line, as shown in Eq. 2:

$$\mathbb{V}_l^* = \{\arg\min \sum_{i \in \mathbb{u}} d_{i,l} \mid \mathbb{u} \subseteq \mathbb{V}_l, |\mathbb{u}| = N_l^*\}, \forall l \in L \tag{2}$$

3.2.2. Traffic flow conflict and coexistence graphs

To develop a collision-free and time-efficient ROW allocation scheme, we decouple the spatial conflict relationships by mapping them onto the temporal dimension.

First, a flow direction conflict graph (FDCG) is introduced to represent the potential interactions of traffic flows in different directions. The FDCG has a static fixed topology, which can be represented in the following form:

$$G_{conflict} = (V, E_{conflict}) \tag{3}$$

$$E_{conflict} = E_{converging} \cup E_{diverging} \cup E_{crossing} \tag{4}$$

where V is the set of all traffic flow directions in the control zone, $E_{conflict}$ denotes the set of conflict relationships between traffic flows.

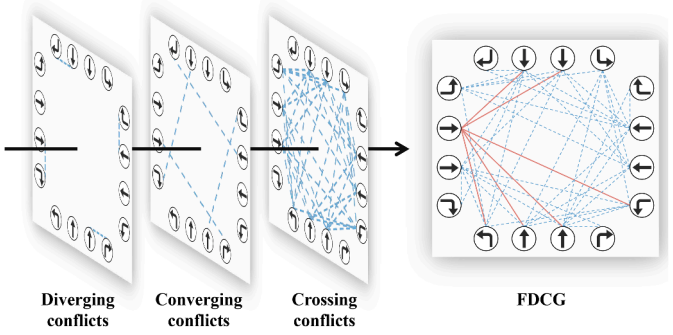

Fig. 3. Illustration of a heterogeneous FDCG.

The conflict relationships between edges include converging, diverging, and crossing conflicts (Chen et al., 2022; Xu et al., 2018). These edges form a heterogeneous FDCG, as is shown in Fig. 3. Traffic flows without edges can pass through the intersection simultaneously. Thus, we use the complementary graph of the FDCG, relative to the fully connected graph, to represent the coexistence of traffic flows:

$$\begin{aligned} G_{coexisting} &= (V, E_{coexisting}) \\ E_{coexisting} &= E \backslash E_{conflict} \end{aligned} \tag{5}$$

where E is the edge of the fully connected graph G. Therefore, it is necessary to satisfy that the traffic flows where vehicles are allowed to pass through the intersection at the same time have edges on $G_{coexisting}$ with each other.

3.2.3. Collaboration based on uncertain behaviors

Based on the conflict and coexistence relationships, risk events may arise from the uncertain behavior of CHVs. For example, when CHVs

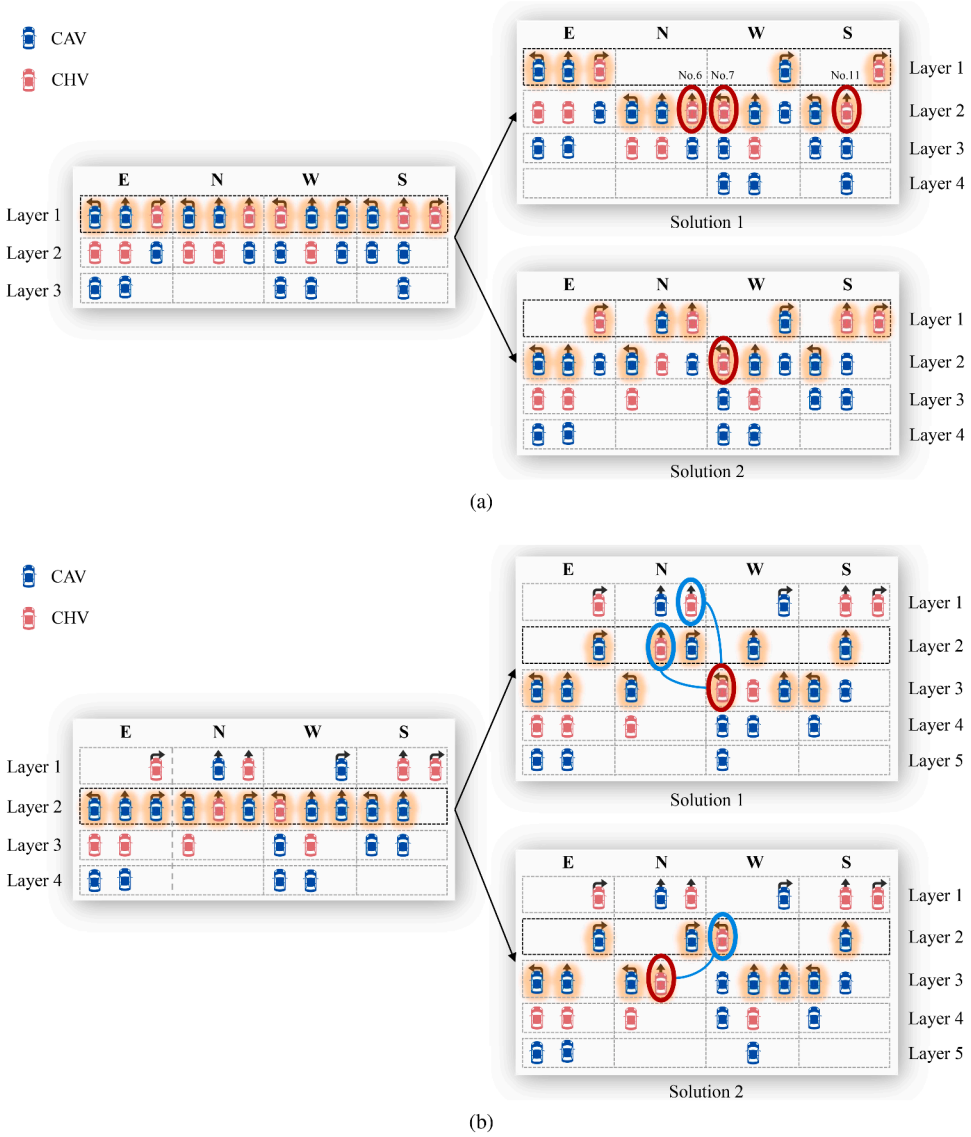

Fig. 4. The examples of two mechanisms. (a) Exposure mitigation. (b) Risk retrospection.

are scheduled to yield the ROW, they may ignore the command due to selfish decision-making. This is referred to as CHV exposure, where the CHV does not follow the vehicle ahead through the intersection. Another potential risk is when CHVs occupy a ROW that they can encroach upon, which could lead to direct interactions at the intersection if one of the CHVs violates the command. These uncontrollable events depend on the individual decision-making of the CHVs, which can reduce passage efficiency and increase safety risks. Therefore, we introduce exposure mitigation to address CHV exposure and risk retrospection to handle dangerous CHV interactions. First, we define the ROW allocation graph to support the two subsequent mechanisms.

Definition 2 (ROW Allocation Graph)**.** A spatio-temporal allocation graph is constructed based on the ROW sequence and lane divisions, where vehicles with the same ROW priority within each lane are grouped into the same layer.

In the control zone, the initial ROW allocation graph is established according to the natural queuing order of vehicles. At this stage, conflicts may exist between candidates in the same layer since no filtering has been applied. Starting from the topmost layer, we filter the candidates to assign vehicles to the same layer that can coexist while maximizing the overall payoff. These filtered vehicles correspond to cliques in graph theory. During this process, exposure elimination is considered:

Definition 3 (Exposure Mitigation)**.** When selecting coexistible vehicles from the candidates, ROW is allocated in a coordinated manner to minimize the occurrence of CHVs exposure.

A simple example of exposure mitigation is illustrated in Fig. 4a. The initial cluster consists of 12 vehicles in layer 1 (i.e., highlighted vehicles). Various combination strategies can be used to select coexisting members:

- Solution 1: Five vehicles are granted the ROW, including three CAVs and two CHVs. The remaining vehicles are deferred to layer 2, waiting for ROW allocation in the next round. This method exposes three CHVs in layer 2, increasing the likelihood of command violations. The probability that all three exposed CHVs comply with the ROW instruction is denoted as $P_1 = \prod_{c\in\{6,7,11\}}(1-\mathbb{E}_c)$, where $\mathbb{E}_c$ denotes the probability that CHV c violates the commends.
- Solution 2: Peer collaboration is applied, prioritizing the minimization of exposed CHVs among the unselected vehicles when determining coexisting members. In this case, six vehicles are granted ROW, including two CAVs and four CHVs. Consequently, only 1 CHV

is exposed in layer 2, and the probability of ROW compliance is $P_2 = 1 - \mathbb{E}_7$.

We assume that CHVs have the same $\mathbb{E}_c$, and obviously $P_1 < P_2$. Thus, exposure mitigation effectively enhances the resilience of ROW allocation by reducing the risk of ROW violations.

Even with the exposure mitigation mechanism in place, some CHVs may still be exposed in the final ROW allocation. This occurs because the primary goal when searching for cliques in the co-existing graph is to maximize passage efficiency, i.e., to maximize the size of the cliques. The exposure mitigation mechanism works by evaluating and ranking candidate cliques based on a weighted method. However, in some cases, cliques containing exposed CHVs may still yield the largest payoff. The clique that satisfies the maximum payoff can be calculated by Eq. 6:

$$C_k = \{\arg\max \left(|\bar{C}| - \sum_{c \in \bar{C}} \delta_c \tau_c \right) \mid \bar{C} \in \mathbb{C}_k\}, \forall k \in \{1, 2, \cdots\} \tag{6}$$

where $\mathbb{C}_k$ represents the set of cliques in the kth layer. The τ_c is a binary variable denoting the type of vehicle c, which takes the value of 1 if vehicle c is a CHV. δ_c is a binary variable that indicates whether vehicle c is exposed.

The issue of exposed CHVs remains unresolved, as they still have the opportunity to encroach on higher-priority ROW, which may belong to CHVs on conflicting routes. This could lead to direct encounters between CHVs at intersections. While social interaction rules can mitigate these conflicts, they introduce additional time delays (Zhou et al., 2022). To address this, the risk retrospection mechanism is introduced.

Definition 4 (Risk Retrospection). When CHVs drop out of the current ROW layer allocation, the previous ROW is retrospected to prevent direct interactions between the dropping CHVs and other CHVs within the intersection.

Similarly, we extend Solution 2 from Fig. 4a to analyze risk retrospection, with the detailed process illustrated in Fig. 4b. Two coexisting member combination solutions are presented for layer 2:

- Solution 1: In this solution, the CHV making a left turn at the west entrance (referred to as the target CHV) relinquishes its ROW and is temporarily assigned to layer 3. This allocation requires the target CHV to wait for vehicles in layers 1 and 2 to pass through the intersection first. However, as the target CHV has no preceding vehicle, it may encroach on the ROW by violating MEC commands. Analyzing the conflict relationships reveals that two CHVs traveling straight from the north entrance could directly interact with the target CHV inside the intersection with a probability of $P_1 = 1 \times \mathbb{E}_c + 1 \times (1 - \mathbb{E}_c)\mathbb{E}_c$.
- Solution 2: Here, the target CHV is a straight-traveling vehicle from the north entrance. Its preceding vehicle is assigned to layer 1, restricting its potential ROW encroachment to layer 2 in the event of a command violation. In this case, only the left-turning CHV from the west entrance in layer 2 could directly interact with the target CHV, with a probability of $P_2 = 1 \times \mathbb{E}_c$.

Clearly, $P_1 > P_2$, indicating that Solution 2 is more effective in minimizing risky interactions caused by the uncertain behavior of CHVs.

Similar to exposure mitigation, risk retrospection cannot entirely eliminate risk interactions for CHVs due to the throughput efficiency of vehicle clusters. We incorporate the risk retrospection mechanism into the payoff function, allowing Eq. 6 to be rewritten as follows:

$$C_k = \{\arg\max \left(|\bar{C}| - \sum_{c \in \bar{C}} \delta_c \tau_c (1 - \sum_{s \in \{e_c, e_c+1, \cdots, k-1\}} |\lambda_c^s|) \right) \mid \bar{C} \in \mathbb{C}_k\}, \forall k \in \{1, 2, \cdots\} \tag{7}$$

$$\lambda_c^s = \{b \in C_s \mid (V_c, V_b) \in E_{conflict}, \tau_b = 1\}, \forall s \in \{e_c, e_c + 1, \cdots, k - 1\} \tag{8}$$

where λ_c^s is the set of CHVs in layer s that may interact directly with vehicle c. e_c is the ROW layer that vehicle c may encroach upon.

3.2.4. Sequential ROW allocation

Algorithm 1 The procedure of the pessimistic estimation-based beam search.

Input: Initial queuing state $\mathcal{N}_0$ of the cluster, ROW allocation scheme $\mathcal{T}_0$
Output: final ROW allocation scheme $\mathcal{T}^*$

```
T_0 ← N_0, s ← 0
while ∀N_s ∈ T_s has child nodes do
    for N_s ∈ T_s do
        expand all child nodes N_{s+1} by selecting potential cliques on FDCG
        T'_s ← N_{s+1}
    end for
    # TED module
    for N_{s+1} ∈ T'_s do
        calculate clique benefit f(C̃_{s+1})
        estimate pessimistic risk P(C̃_{s+1})
        normalize benefit F(C̃_{s+1}) = (f(C̃_{s+1}), P(C̃_{s+1}))
    end for
    K ← random[2, 4], K ∈ Z^+
    select nodes with top-K scores in T'_s
    T_{s+1} ← {N^0_{s+1}, N^1_{s+1}, ··· , N^K_{s+1}, }
    s ← s + 1
end while
T* ← argmax_{N_s ∈ T_s} F(N_s)
```

The above collaborations will act as soft constraints to guide the generation of feasible solutions. Given that ROW allocation is a Markov decision process, beam search algorithm can address this issue online.

Beam search is a heuristic algorithm commonly used in large search spaces, particularly in natural language processing (Kuroiwa & Beck, 2024; Ting & Wu, 2017; Xie et al., 2024). It strikes a balance between search performance and computational cost by selectively expanding only the most promising nodes while discarding others. In traditional beam search, each round's solution does not account for future cases. That is, relying on previous solutions may lead to a tactical trap–where an allocation scheme with high benefits in earlier rounds results in lower benefits later on (Świechowski et al., 2023). To more accurately evaluate ROW allocation solutions, we introduce the pessimistic estimation-based beam search (PEBS).

The concept of PEBS is structured in Fig. 5. The initial queue state of the vehicle cluster serves as the root node. Starting from this root, the tree is expanded layer by layer by identifying potential cliques on the FDCG. Each child node represents a distinct ROW allocation solution. At each layer, the sub-nodes are evaluated by the Trap-Escape Decision (TED) module, which selects the partial solution with the highest potential benefit for further exploration.

The TED module comprises two components: current clique benefit computation and pessimistic estimation. The first calculates the current benefits of solutions. The second incorporates worst-case scenarios of CHV violations, adjusting prior benefits downward to account for these risks. Specifically, it assumes that any CHV may violate commands, with a probability $\mathbb{E}_c$. The probability of a violation for forward-looking solutions can be written as Eq. 9:

$$P(\widetilde{C_k}) = \prod_{c=1}^{\widetilde{C_k}} \tau_c (1 - \mathbb{E}_c) \tag{9}$$

where $\widetilde{C_k}$ is the candidate clique for layer k.

To mitigate overemphasis on immediate benefits, the TED module adjusts the benefit $f(P(\widetilde{C_k}))$ using the prospective pessimistic estimate $P(\widetilde{C_k})$. Sub-nodes in each layer are ranked by their adjusted scores, and the top K solutions (beam width) are carried forward to the next layer. To enhance solution diversity, K is randomized in each iteration, controlling the pruning scale (Tam et al., 2024). The search terminates once

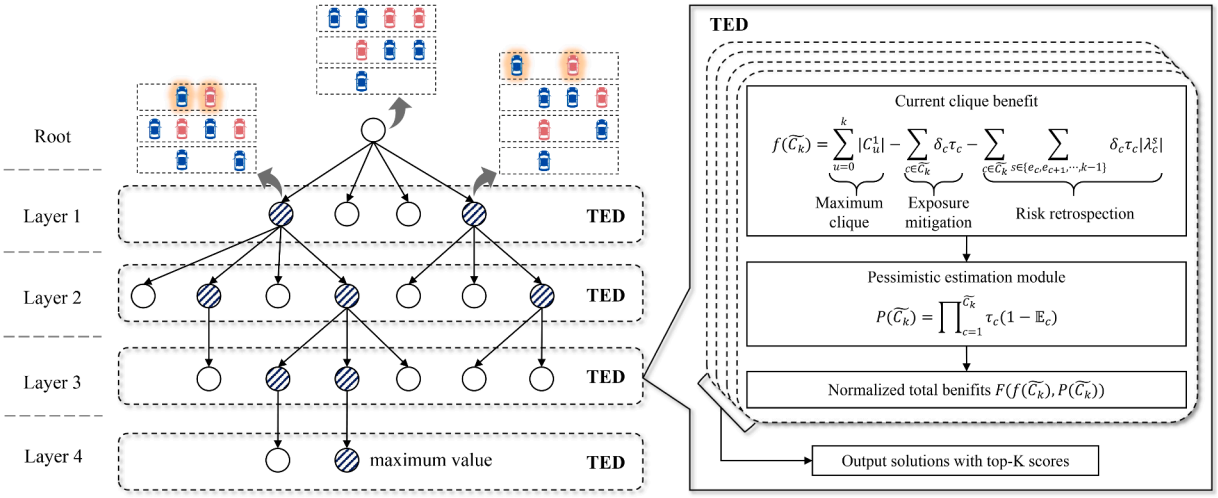

Fig. 5. The process of pessimistic estimation-based beam search.

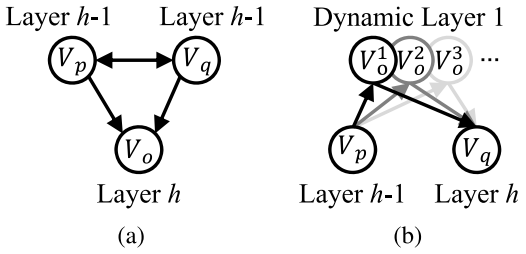

Fig. 6. Illustration of two motifs. (a) Motif-1 with a fixed structure. (b) Motif-2 with dynamic switching structures.

all vehicles are assigned ROW, yielding the solution with the highest overall score. Note that if the node is not expandable, we make itself a child node for comparison with other expandable nodes. The algorithm 1 is a description of the PEBS procedure.

3.3. Middle level: Communication networking

First, we filter effective interaction objects based on the ROW allocation scheme. Next, we construct the network motif according to the information flow of ROW. We then propose static networking and dynamic link updating methods to build a reliable communication topology.

3.3.1. Filter effective interaction objects

From a system perspective, the ego vehicle waits for all vehicles in the upper layer to pass through the intersection before obtaining ROW. However, not all of these vehicles conflict with the ego vehicle, so information sharing between conflict-free vehicles is unnecessary. Thus, we filter interactions based on internal conflict points, retaining only vehicles with path conflicts as information sources and destinations. This reduces redundant information transmission and lowers communication bandwidth consumption. We add communication demand pairs to set $\mathbb{D}$ by Eq. 10.

$$\mathbb{D} = \{(V_p, V_q) | (V_p, V_q) \in G_{conflict}\}, \forall V_p \in \mathcal{T}^*_{h-1}, V_q \in \mathcal{T}^*_h, h = 1, 2, \cdots, |\mathcal{T}^*| \tag{10}$$

where $\mathcal{T}^*_s$ represents the set of vehicles included in the clique at layer s of the ROW allocation scheme.

3.3.2. Motifs in communication networks

Motifs serve as fundamental blocks in networks, typically comprising a small number of nodes (Milo et al., 2002). They provide redundant pathways to enhance fault tolerance. To balance structural simplicity and functionality, we utilize 3-node motifs–commonly employed in existing research–to construct the backbone network (Liu et al., 2020; Qiu et al., 2022; Roy et al., 2022). Specifically, we implement heterogeneous directed-edge 3-node motifs tailored to different combinations of interacting vehicles.

(1) Motif-1 for line-of-sight (LOS) conditions

Unidirectional edges ensure direct information flow from upper-layer vehicles to lower-layer vehicles under normal conditions, while bidirectional edges link vehicles within the same layer to mitigate edge failures via multi-hop communication. Fig. 6a illustrates the motif-1 governing upper- and lower-layer interactions. The adjacency matrix of the motif-1 is expressed as:

$$M^1_{\{V_p,V_q,V_o\}} = \begin{bmatrix} 0 & 1 & 1 \\ 1 & 0 & 1 \\ 0 & 0 & 0 \end{bmatrix}, \forall (V_p, V_o), (V_q, V_o) \in \mathbb{D}, \{V_p, V_q, V_o\} \in \mathbb{H}_{LOS} \tag{11}$$

where $\mathbb{H}_{LOS}$ is the set of vehicles that satisfy the LOS condition. Motif-1 is employed to construct fixed minimal network components that capture the continuous interaction demands among three vehicles during the cluster's passage through the intersection. Multiple stable motif-1 structures are embedded into the communication network, collectively forming a static backbone topology. The three vehicles applying motif-1 must satisfy the requirements of **Rule 1**:

Rule 1. *The interactions where $M^1_{V_p,V_q,V_o}$ applies can be summarized as follows: (i) Vehicles V_p and V_q both have route conflicts with vehicle V_o. (ii) The ROWs of vehicles V_p and V_q are higher than that of vehicle V_o. (iii) Vehicles V_p, V_q, and V_o are positioned in the same or opposite entrance lanes under LOS conditions.*

(2) Motif-2 for non line-of-sight (NLOS) conditions

NLOS shading at intersections weakens the edges of the motifs. For example, when vehicles from adjacent layers are positioned at the north and east entrances, their direct links are obstructed by buildings and trees, causing significant signal fading or even complete link disruption. To address this, we propose the motif-2 to establish communication links, as illustrated in Fig. 6b. Specifically, we use vehicles located near the intersection's interior as relay nodes, enabling a two-hop transmission. The adjacency matrix for motif-2 is shown in Eq. 12:

$$M^2_{\{V_p,V_o,V_q\}} = \begin{bmatrix} 0 & 1 & 0 \\ 0 & 0 & 1 \\ 0 & 0 & 0 \end{bmatrix},$$
$$\forall (V_p, V_q) \in \mathbb{D}, \{V_p, V_o\}, \{V_o, V_q\} \in \mathbb{H}_{LOS}, \{V_p, V_q\} \in \mathbb{H}_{NLOS} \tag{12}$$

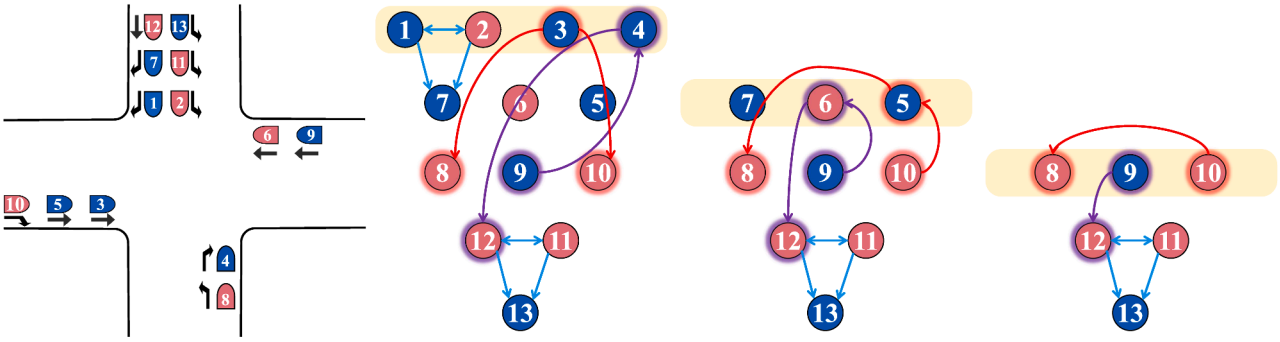

(a) Vehicle distribution. (b) Release of vehicles in Layer 1. (c) Release of vehicles in Layer 2. (d) Release of vehicles in Layer 3.

Fig. 7. Working principle of the dynamic-static coupling network. Blue edges and their corresponding nodes represent motif-1-based minimal network components, such as vehicles 1, 2, 7 and 11, 12, 13. Red edges and their corresponding nodes represent motif-2-based minimal network components, such as vehicles 4, 9, 12. The former constitutes a static structure that is maintained and executed throughout the entire process, whereas the latter forms a dynamic structure in which relay nodes are assigned at each ROW layer and switch sequentially with the release order.

where $\mathbb{H}_{NLOS}$ is the set of vehicles that satisfy the NLOS condition. The relay nodes in motif-2 adapt dynamically to the sequential passage of high-priority vehicles through the intersection. This mechanism leverages the layered release process of the ROW scheme, whereby the identity of relay nodes is switched in real time to ensure that message propagation routes consistently bypass occlusions. As a result, the minimal network components generated by motif-2 are inherently dynamic, with node roles changing over time. When these motif-2-based components are integrated into the backbone, a dynamic network topology with time-stamped labels spontaneously emerges. The invocation of motif-2 is conditioned on the satisfaction of **Rule 2**.

Rule 2. *Three vehicles meeting the following conditions can be connected using* $M^2_{V_p,V_o,V_q}$*: (i) Vehicles* V_p *and* V_q *have path conflicts. (ii) The ROW priority of the vehicles satisfies* $ROW(V_o) > ROW(V_p) > ROW(V_q)$*. (iii) There is an NLOS condition between vehicles* V_p *and* V_q*. (iv) Vehicle* V_o *is one of the highest-priority vehicles that has not yet passed through the intersection, meaning it is dynamically selected.*

3.3.3. Dynamic-static coupling network based on motifs

Once communication demands and potential occlusions are identified, motif-1 and motif-2 are employed to construct minimal network components between interacting vehicles, which are then assembled to generate a dynamic-static coupling network. For interacting vehicles under LOS conditions, communication links remain stable throughout the cluster's passage through the intersection; thus, motif-1 is used to form the corresponding minimal components. By contrast, vehicles under NLOS conditions require relay nodes to bypass occlusions, for which motif-2 is applied. The detailed construction procedure is shown in Algorithm 2. We further explain the networking principles:

- **Step 1.** Combine the ROW assignment scheme with flow directions at the intersection to identify vehicle pairs set $\mathbb{D}$ with communication demands by Eq. 10.
- **Step 2.** Add edges between LOS vehicles in pair to form the backbone network:

$$\boldsymbol{A}_{V_p,V_q} = \begin{cases} 1, & \text{if } \{V_p,V_q\} \in \mathbb{H}_{LOS} \\ 0, & \text{o.w.} \end{cases}, \forall (V_p,V_q) \in \mathbb{D} \tag{13}$$

  where $\boldsymbol{A}_{V_p,V_q}$ is a binary variable that equals 1 if there exists a link between vehicle V_p and vehicle V_q, and 0 otherwise. At this stage, the backbone may be fragmented, as routing paths for NLOS pairs have not yet been established.
- **Step 3.** For vehicle pair $(V_p,V_o) \in \mathbb{D}$ already connected in the backbone, if another pair $(V_q,V_o) \in \mathbb{D}$ satisfies **Rule 1**, motif-1 is established among the three vehicles according to Eq. 11. The minimal component generated by motif-1 is then integrated into the backbone:

$$\boldsymbol{A}_{static} = \boldsymbol{A} + \sum_{\substack{(V_p,V_o),(V_q,V_o)\in\mathbb{D} \\ \{V_p,V_q,V_o\}\in\mathbb{H}_{LOS}}} f_{N_G}(M^1_{\{V_p,V_q,V_o\}}) \tag{14}$$

  where $f_{N_G}(\cdot)$ denotes embedding the motif matrix into the global adjacency matrix.The resulting backbone is static, as its edges persist throughout the operation of vehicles (see Fig. 7).
- **Step 4.** For vehicle pair $(V_p,V_q) \in \mathbb{D}$ with communication demands but no direct edges, if **Rule 2** is satisfied, motif-2 is employed to construct minimal components by selecting appropriate relay nodes $V_o^h \in \mathbb{D}, 0 < h < |\mathcal{T}^*(V_p)|\}$. Relay nodes are dynamically chosen at each ROW layer among vehicles in LOS conditions (e.g., adjacent or located within the intersection), following the principle of minimum node degree. This design choice is motivated by our previous findings that using relay nodes with the minimum node degree for message forwarding can effectively defend against potential malicious network attacks (Wu et al., 2024b). It facilitates the formation

Algorithm 2 The procedure of dynamic-static coupling networking.

Input: ROW allocation scheme $\mathcal{T}^*$, FDCG $G_{conflict}$
Output: The adjacency matrices $\boldsymbol{A}_{static}$ and $\boldsymbol{A}^h_{dynamic}$

use Eq. 10 to establish the effective communication demands set $\mathbb{D}$
# build the basic edges of the network
for $(V_p,V_q) \in \mathbb{D}$ **do**
  if $\{V_p,V_q\} \in \mathbb{H}_{LOS}$ and $\boldsymbol{A}_{V_p,V_q} = 0$ **then**
    $\boldsymbol{A}_{V_p,V_q} \leftarrow 1$
  end if
end for
# use motif-1 to strength static backbone network
for $(V_p,V_o),(V_q,V_o) \in \mathbb{D}$ **do**
  if $\{V_p,V_q,V_o\} \in \mathbb{H}_{LOS}$ **then**
    update $\boldsymbol{A}_{static}$ by Eq. 11, 14
  end if
end for
# use motif-2 to generate dynamic temporal network
while $h < |\mathcal{T}^*|$ **do**
  for $(V_p,V_q) \in \mathbb{D}$ **do**
    if $\{V_p,V_q\} \in \mathbb{H}_{NLOS}$ and $h < |\mathcal{T}^*(V_p)|$ **then**
      select vehicle V_o^h from $\mathcal{T}_h^*$ with the minimum node degree by Eq. 15
    end if
  end for
  update $\boldsymbol{A}^h_{dynamic}$ by Eq. 12, 16
  $h \leftarrow h+1$
end while

of a more robust communication network. The explicit formulation is as follows:

$$V_o^h = \arg \min_{\substack{V_o \in \mathcal{T}_h^* \\ h \in [1, |\mathcal{T}^*(V_p)|-1]}} \sum_{V \in N_G} \boldsymbol{A}^*_{V,V_o} \tag{15}$$

where h denotes the ROW layer depth. V_o^h denotes the relay node selected at layer h. Each V_o is a member of the vehicle set $\mathcal{T}_h^*$ at layer h. V_p represents the vehicle in the pair with the higher ROW layer, and V denotes a vehicle in the cluster. $\boldsymbol{A}^*$ is the temporary adjacency matrix used to compute node degrees. We define a node's degree as the total number of directed edges pointing to it. At the initial moment, $\boldsymbol{A}^* = \boldsymbol{A}_{static}$. Whenever V_o^h is selected as the relay node for $\{V_p, V_q\}$, $\boldsymbol{A}^*_{V_p,V_o}$ is incremented by 1 to update the node's in-degree. For each relay node, directed edges are established with vehicles in the pair according to Eq. 12, and they will be added to the dynamic network:

$$\boldsymbol{A}^h_{d\,ynamic} = \sum_{\substack{(V_p,V_q)\in\mathbb{D} \\ \{V_p,V_q\}\in\mathbb{H}_{NLOS} \\ \{V_p,V_o^h\},\{V_o^h,V_q\}\in\mathbb{H}_{LOS}}} f_{N_G}(M^2_{\{V_p,V_q,V_o^h\}}) \tag{16}$$

As minimal components generated by motif-2 are time-sensitive, they are updated after each ROW layer is released, thereby forming the dynamic portion of the network (illustrated in Fig. 7).

- **Step 5.** The communication scheme derived from the dynamic-static coupling network is then distributed to vehicles for execution. The network is updated iteratively until the next ROW assignment is generated.

3.4. Lower level: Local trajectory planning

For each ego vehicle in the cluster, a trajectory planning model can be constructed locally and solved using DMPC within a rolling horizon framework. CAVs execute actions unconditionally, while CHVs decide based on their willingness to comply. If CHVs distrust the instructions, their behavior is modeled using the approach introduced in (Fang et al., 2024).

3.4.1. Local safety gap modeling

We propose a spatio-temporal embedded safety gap model to improve the fault-tolerance of the strategy.

- **Objective function**

The objective of the proposed framework is to design a collision-free trajectory that ensures the ego vehicle can traverse the intersection in the shortest possible time, immediately following a neighboring vehicle with higher ROW priority. To achieve this, the objective function is formulated to minimize the distance between each vehicle's position $X_{i,l}(u|t)$ and its designated destination $r_{i,l}$.

$$\textbf{min} \sum_{u\in[0,\Delta T_H]} (r_{i,l} - X_{i,l}(u|t)) \tag{17}$$

where t represents the current moment and ΔT_H denotes the planning horizon for trajectory optimization.

- **Dynamics constraints**

First, the constraints for the vehicle's general longitudinal motion are tailored as follows:

$$X_{i,l}(u+1|t) = X_{i,l}(u|t) + v_{i,l}(u|t)\Delta u + \frac{1}{2}a_{i,l}(u|t)\Delta u^2, \forall i \in N_l^*, u \in [0, \Delta T_H] \tag{18}$$

$$v_{i,l}(u+1|t) = v_{i,l}(u|t) + a_{i,l}(u|t)\Delta u, \forall i \in N_l^*, u \in [0, \Delta T_H] \tag{19}$$

$$a_{min} \le a_{i,l}(u|t) \le a_{max}, \forall i \in N_l^*, u \in [0, \Delta T_H] \tag{20}$$

Constraints 18 and 19 update the ego vehicle's position and speed at each time step, respectively. Constraint 20 establishes the upper and lower bounds for acceleration. Δu is the decision step length.

- **Updating the state information of neighboring vehicles**

Vehicles share state information $W(u|t) = \{X(u|t), v(u|t), a(u|t)\}$ over the communication network. However, signal noise interference may lead to packet loss. Although retransmissions can mitigate this, they may cause the transmission delay to exceed the tolerance threshold ΔT_{th} of control task. If the delay exceeds this threshold, the message packet is discarded. In this case, the ego vehicle will make decision on historical information. The neighbor state information is updated according to Eq. 21:

$$W_j(u|t+1) = \begin{cases} W_j^*(u|t+1), & \text{if } o(path_{m,n}) \le \Delta T_{th} \\ W_j(u+1|t), & \text{o.w.} \end{cases}, \forall i \in N_l^*, j \in N_h^*, u \in [0, \Delta T_H] \tag{21}$$

where $W_j^*(u|t+1)$ represents the most recent state information from the neighbor vehicle j at time $t+1$. The total transmission delay between vehicles i and j, $o(path^t_{i,j})$, is given by Eq. 22. The transmission delay for a single-hop communication link is computed using Eq. 23, where $q_{e^t_{m,n}}$ is the total number of message packets for edge $e_{m,n}$, and $\mathcal{S}^p$ is the standard size of a single message packet. Eq. 24 describes the transmission rate of the communication link between vehicles, where $d^t_{m,n}$ is the Euclidean distance between vehicles m and n at time t, B is the allocated communication bandwidth, and P_V and N_0 denote the transmission power and thermal noise power, respectively (Liu et al., 2022a). Eq. 25 expresses the packet delivery rate as a function of a Gaussian random variable, with r representing the transmission range in the absence of shadowing.

$$o(path^t_{i,j}) = \sum_{e^t_{m,n}\in path^t_{i,j}} o(e^t_{m,n}), \forall m, n \in N \tag{22}$$

$$o(e^t_{m,n}) = \frac{q_{e^t_{m,n}}\mathcal{S}^p}{c^t_{m,n}\mathcal{P}^t_{m,n}}, \forall m, n \in N, e^t_{m,n} \in \boldsymbol{A} \tag{23}$$

$$c^t_{m,n} = B\log_2[1 + \frac{P_V}{N_0(d^t_{m,n})^2}], \forall m, n \in N \tag{24}$$

$$\mathcal{P}^t_{m,n} = Pr\{P^w(d^t_{m,n}) \ge P^w_{min}\} = \int_{10\alpha\log_{10}(\frac{d^t_{m,n}}{r})}^{\infty} \frac{1}{\sqrt{2\pi}\sigma} e^{-\frac{x^2}{2\sigma^2}} dx = Q(\frac{10\alpha}{\sigma}\log_{10}(\frac{d^t_{m,n}}{r})) \tag{25}$$

- **Spatial safety gaps model**

The ego vehicle models its trajectory by considering the spatial safety gaps (SSG) relative to its neighboring vehicles, which are part of the finite conflict object set identified earlier. This method simplifies the optimization problem by reducing the number of interacting objects, thereby decreasing the dimensionality of the variables. Importantly, within the constraints of the ROW hierarchy, the ego vehicle ensures that neighboring vehicles pass the conflict point first. The constraints are set as follows.

$$(F_{l,h} - X_{i,l}(u|t)) - (F_{h,l} - X_{j,h}(u|t)) \ge D_{safe} + M(1 - \delta^1_{i,l}(u|t)\delta^2_{j,h}(u|t)), \forall i \in N_l^*, j \in N_h^*, u \in [0, \Delta T_H] \tag{26}$$

$$F_{l,h} - X_{i,l}(u|t) \ge M(\delta^1_{i,l}(u|t) - 1), \forall i \in N_l^*, u \in [0, \Delta T_H] \tag{27}$$

$$F_{h,l} - X_{j,h}(u|t) \ge M(\delta^2_{j,h}(u|t) - 1), \forall j \in N_h^*, u \in [0, \Delta T_H] \tag{28}$$

$$\delta^1_{i,l}(u|t), \delta^2_{j,h}(u|t) \in \{0,1\}, \forall i \in N_l^*, j \in N_h^*, u \in [0, \Delta T_H] \tag{29}$$

where $F_{l,h}$ and $F_{h,l}$ represent the locations of the conflict points, respectively. M is a sufficiently large constant. When neither the ego vehicle nor the neighboring vehicle has passed the conflict point, they must

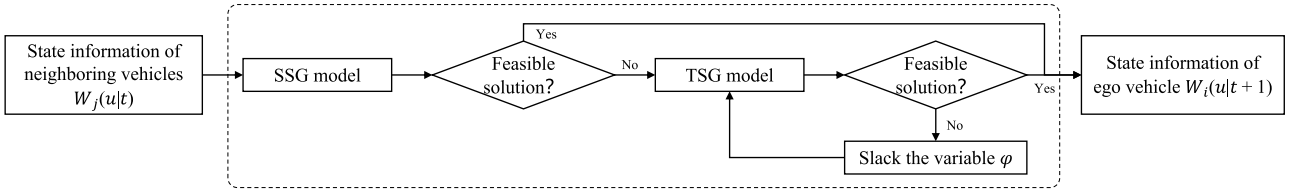

Fig. 8. The framework of STESG.

maintain a safe distance D. Once the neighboring vehicle passes the conflict point, this constraint is lifted. This ensures that the ego vehicle is not influenced by the downstream behavior of the neighboring vehicle, allowing it to focus solely on the most immediate collision risk.

The SSG optimization can be formalized as problem P1. It is a mixed integer linear programming (MILP) problem, which can be solved by commercial solvers:

objective: Eq.(17)

subject to: Eqs.(18) – (20), (26) – (29)

- **Temporal safety gaps model**

It is important to note that a feasible solution for SSG optimization may not always exist. If CHVs deviate from the prescribed commands, a change in right-of-way (ROW) priority may occur, as detailed in the next section. Specifically, when a higher-priority neighboring vehicle concedes ROW to the ego vehicle, the safe distance constraint may no longer be satisfied, i.e., $(F_{l,h} - X_{i,l}(u|t)) - (F_{h,l} - X_{j,h}(u|t)) < D_{safe}$. To address this, we introduce the constraints of temporal safety gaps (TSG) to plan the optimal trajectory, as shown in Eq. 30.

$$\frac{F_{l,h} - X_{i,l}(u|t)}{v_{i,l}(u|t)} - \frac{F_{h,l} - X_{j,h}(u|t)}{v_{j,h}(u|t)} + \varphi_{i,l}(u|t) \geq T_{gap} \tag{30}$$

$$0 \leq \varphi_{i,l}(u|t) \leq \varphi_{i,l}^{max}, \forall i \in N_l^*, u \in [0, \Delta T_H] \tag{31}$$

where T_{gap} represents the time-to-collision threshold, which ensures the safety of interacting vehicles in the time domain. Given the kinematic constraints, it require an iterative process to ensure that the trajectories of ego vehicles converge to satisfy Eq. 30. To facilitate this, we introduce a penalty variable, $\varphi_{i,l}(u|t)$, as defined in Eq. 30, which specifies its allowable range. Importantly, $\varphi_{i,l}(u|t)$ adjusts the degree of relaxation based on the feasibility gradient of the solution, preventing the optimization from prematurely operating in a relaxed space. To incorporate this process, we redefine the objective function of the TSG.

$$\textbf{min} \sum_{u \in [0, \Delta T_H]} (r_{i,l} - X_{i,l}(u|t)) + \sum_{u \in [0, \Delta T_H]} M \varphi_{i,l}(u|t) \tag{32}$$

We define Problem $P2$ to implement the TSG optimization. Notably, Eq. 30 exhibits nonlinear characteristics, making $P2$ a nonlinear planning problem. Such problems are well-suited for solution using Sequential Least Squares Programming (SLSQP), which has been extensively applied in related research (Dubey et al., 2024; Song et al., 2023).

objective: Eq.(32)

subject to: Eqs.(18) – (20), (30), (31)

3.4.2. DMPC Based on rolling horizon

The ego vehicle decomposes centralized tasks into local subtasks for individual trajectory planning, with each subtask modeled using a spatio-temporal embedded safety gap (STESG), as illustrated in Fig. 8. Given the high computational demands of vehicle trajectory planning, a distributed computing method is employed to mitigate complexity. Furthermore, the need for dynamic responsiveness to environmental changes results in a brief information lifecycle, necessitating frequent trajectory updates to maintain this adaptability. To address these challenges, we propose a DMPC framework based on rolling horizon, with the method details provided in Algorithm 3.

Algorithm 3 The solution procedure of the spatio-temporal embedded safety gap model.

Input: ROW allocation scheme $\mathcal{T}^*$, The adjacency matrix $\boldsymbol{A}$ of the communication network

Output: The state information $W_i^*(u|t+1)$ of vehicle i

1: initialize the prediction horizon T_H, the initial state information $W(u|t_0)$, $u = 0$
2: For each vehicle $i \in \mathcal{T}^*$
3: **while** $X_{i,l} < p_{i,l}$ **do** #$p_{i,l}$ is the position where vehicle i leaves the intersection
4: **for** $j \in \mathbb{D}_i$ **do**
5: update $W_j(u|t+1)$ by Eqs. 21–24
6: **end for**
7: establish SSG model and solve Problem P1
8: **if** $W_i(u|t+1) \in \varnothing$ **then**
9: establish TSG model and solve Problem P2
10: **if** $W_i(u|t+1) \in \varnothing$ **then**
11: slack the variable φ and return to line 9
12: **end if**
13: **end if**
14: update $W_i^*(u|t+1)$
15: implement the optimal action for the first step $W_i^*(1|t+1)$
16: send $W_i^*(u|t+1)$ to its neighboring vehicle j
17: $t \leftarrow t+1$
18: **end while**

3.5. Re-computation checker

Uncertain behaviors can lead to disruptions in the orderly execution of the ROW allocation scheme. To address this problem, the re-computation checker is designed to monitor and identify disordered vehicles and the vehicles affected by cascading disruptions, enabling the quick restoration to an orderly state. In essence, the re-computation checker enhances the resilience of the proposed method.

This mechanism leverages newly defined social interaction rules for vehicles, which is inspired by (Zhou et al., 2024, 2022). We establish conflict-oriented judgment conditions for emergency braking.

$$\Delta L_{i,l} = F_{l,h}^{(1)} - \frac{(v_{stop})^2 - (v_{i,l}(0|t))^2}{2a_{min}} \tag{33}$$

where $F_{l,h}^{(1)}$ denotes the location of the first conflict point on vehicle i's route l within the intersection. The distance $\Delta L_{i,l}$ represents the remaining distance to $F_{l,h}^{(1)}$ after vehicle i brakes at maximum deceleration. $\Delta L_{i,l}$ quantifies the vehicle's ultimate collision avoidance capability under emergency conditions By evaluating $\Delta L_{i,l}$ for vehicles navigating the intersection, we propose two propositions for segregating vehicles in turbulent traffic scenarios.

Proposition 1. *If the target vehicle can yield to participate in ROW reallocation ($\Delta L_{i,l} > 0$), it is added to the recalculation set $\mathbb{B}_R$; otherwise, it is assigned to the continuation set $\mathbb{B}_C$.*

Proposition 2. *The CHVs in $\mathbb{B}_R$ that violate commands are assigned the highest-priority ROW in the new scheme, while vehicles in $\mathbb{B}_C$ proceed according to the original scheme.*

Table 1
Vehicle arrival rate scenario settings.

Scenario	Through demand (dedicated) (veh/h/lane)	Through demand (mixed) (veh/h/lane)	Left demand (veh/h/lane)	Right demand (veh/h/lane)
1	400	80	360	360
2	500	100	400	400
3	700	140	480	480

Table 2
Parameter values.

Notations	Values	Notations	Values	Notations	Values	Notations	Values
Δu	0.2 s	ΔT_{th}	50 ms	$a_{\min}$	-4 m/s^2	$a_{\max}$	4 m/s^2
$v^s_{\max}$	11.11 m/s	D_{safe}	6 m	T_{gap}	1.5 s	$p_{i,l}$	215 m
N_G	60 veh	r	150 m	N_0	-96 dBm	P_V	20 dBm
B	5 MHz	S^p	32 KB	$r_{i,l}$	400 m	ΔT_H	4 s

Table 3
Real vehicle arrival rate for CG-JN intersection.

Vehicle type	Vehicle arrival rate (veh/h)											
	N-S	N-E	N-W	S-N	S-W	S-E	W-E	W-N	W-S	E-W	E-S	E-N
Car	376	473	677	316	228	332	1684	375	236	857	283	776
Bus	31	19	6	16	17	0	9	4	11	9	10	0
Truck	3	9	7	4	15	11	52	14	8	5	31	15

The re-computation checker resolves disordered passing orders and redistributes the ROW based on propositions 1 and 2. It assumes that CHVs violating commands will yield to vehicles in the continuation set. This assumption is consistent with social interaction norms, as drivers are unlikely to preempt vehicles that cannot brake. After the re-computation check, the updated vehicle cluster awaiting allocation is processed through the proposed three-level model to compute a revised scheme.

4. Experiments and results

4.1. Setup

4.1.1. Basic parameter settings

A typical four-arm unsignalized intersection is considered, featuring three lanes at each entrance and exit. The designated flow directions for each lane and the conflict points within the intersection are clearly labeled in Fig. 1. To reflect real-world conditions, the right entrance lanes accommodate a mix of straight and right-turn movements. The length of control zone is set to 200 m. We assume the length of all vehicles is 4 m.

Since unsignalized intersections are generally suitable for low-traffic scenarios, the experiments were designed to include both heavy and light traffic demands. The market penetration rate (MPR) of CAVs is set at 50%, 70%, and 90% for the assumption of high-MPR mixed traffic scenarios. Besides, we set the vehicle violation rate (VVR) of CHVs as 0, 0.2, 0.4, 0.6, and 0.8. The vehicle arrival rates and simulation parameters are detailed in Tables 1 and 2, respectively (Wu et al., 2024b,c). To assess the applicability of the proposed framework under realistic conditions, simulation experiments were conducted using two representative types of high-demand urban intersections. The first test site is the Changgang Road-Jiangnan Avenue (CG-JN) intersection in Guangzhou, representing a skewed junction with non-orthogonal approaches that often induce complex traffic interactions. The second is a T-shaped intersection at Qinglong Street and Renmin Middle Road (QL-RM) in Chengdu. Fig. 9 illustrates the real-world road networks, their corresponding simulation models, and the FDCG representations, with lane configurations and flow directions fully aligned with field conditions. Both intersections are signalized in reality but were configured as unsignalized in the simulation in order to evaluate the performance of the proposed framework under unsignalized intersection management, while keeping all other settings consistent with the real-world environment.

Table 4
Real vehicle arrival rate for QL-RM intersection.

Vehicle type	Vehicle arrival rate (veh/h)					
	N-S	N-W	S-N	S-W	W-N	W-S
Car	697	297	453	644	307	960
Bus	9	19	17	14	15	7
Truck	12	6	11	33	4	31

Traffic demand was derived from one hour of morning-peak observations. Specifically, data for the CG-JN intersection were collected from 8:30 to 9:30 a.m. on May 19, 2023, while data for the QL-RM intersection were collected from 7:00 to 8:00 a.m. on April 11, 2023. These datasets were obtained from Automatic Vehicle Identification (AVI) checkpoints, and detailed traffic demand configurations are summarized in Tables 3 and 4. To capture vehicle heterogeneity, buses and trucks were explicitly modeled in SUMO using the built-in motion models, with vehicle lengths set to 10 m and 8 m, respectively. Vehicle arrivals followed a Poisson process, and other simulation parameters were configured in accordance with Table 2.

Traffic-level simulations were carried out using the SUMO (Simulation of Urban MObility) platform, while communication-level dynamics were evaluated through numerical simulations. To more realistically capture the driving fluctuations of CHVs, Gaussian noise with a mean of 0 and a standard deviation of 0.1 m/s was added to their desired speed during the simulation. All experiments were implemented in Python on a desktop computer equipped with an Intel Core i5-13600KF processor (3.50 GHz base frequency) and 32 GB of RAM.

4.1.2. Comparison methods

To validate the effectiveness of the proposed method, two benchmark approaches were selected for comparison. Both were originally designed for unsignalized intersections and can be extended to mixed traffic scenarios. The first focuses on controlling individual vehicles, pursuing the maximization of traffic efficiency under fully rational vehicle behavior, whereas the second allocates ROW through platoon-based organization, completely eliminating the possibility of CHV violations. Our method lies between the two, leveraging flexible individual-vehicle arrangements to balance an efficient ROW scheme with a low probability of violations. For fairness, the benchmark methods and the proposed FTC were configured with identical parameter settings.

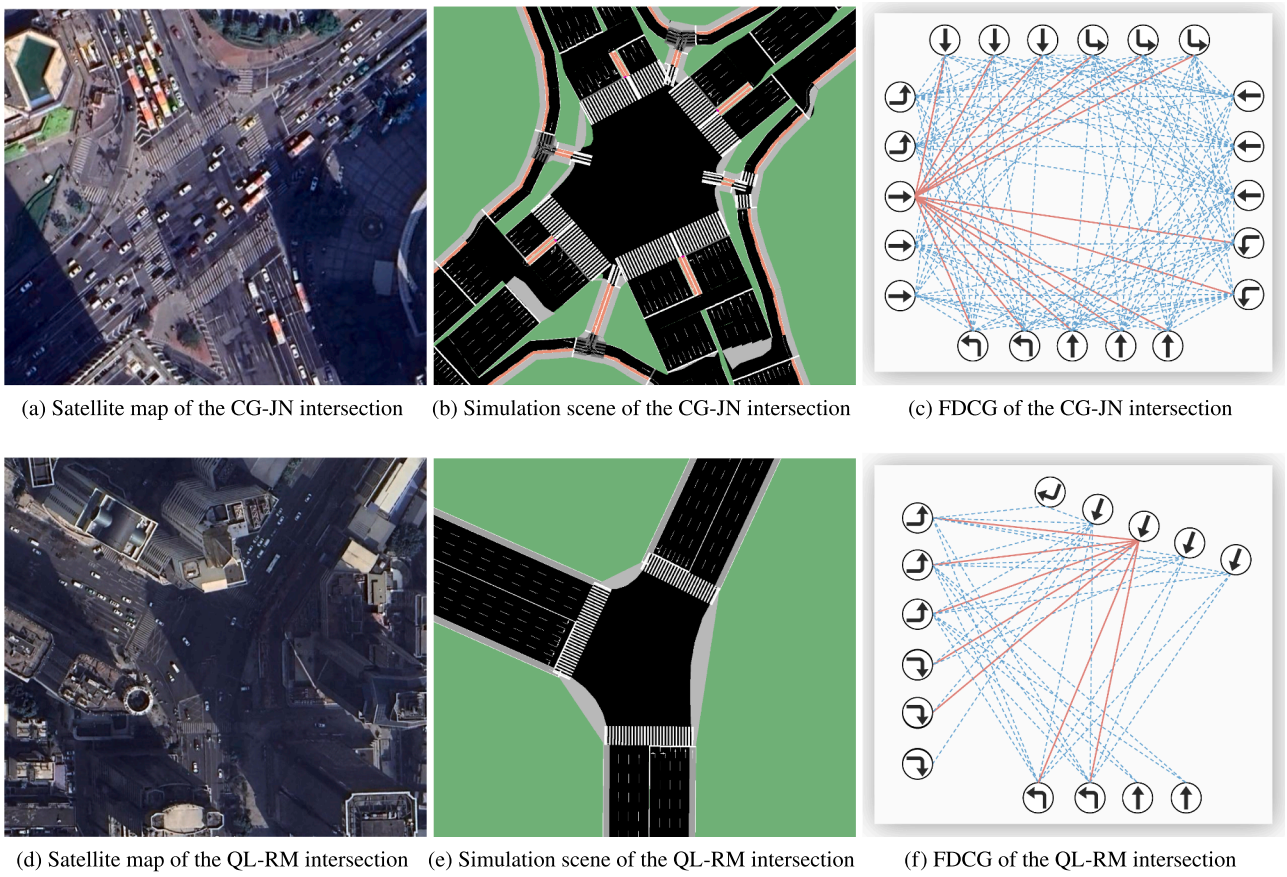

(a) Satellite map of the CG-JN intersection (b) Simulation scene of the CG-JN intersection (c) FDCG of the CG-JN intersection

(d) Satellite map of the QL-RM intersection (e) Simulation scene of the QL-RM intersection (f) FDCG of the QL-RM intersection

Fig. 9. Configuration of two types of real-world intersections.

- **MCC** (Chen et al., 2022): This method is graph-theory-based and proposes a decoupling approach to resolve multi-vehicle behavioral conflicts at intersections. In terms of ROW assignment, the minimum clique cover method is employed to determine vehicle passing sequences. When a CHV violates commands, cascading vehicles whose ROW is encroached are required to decelerate and yield, while the violating CHV is temporarily granted the highest-priority ROW. For communication, a Predecessor-Leader Following (PLF) static topology is adopted to facilitate information exchange among vehicles. At the control level, a linear feedback controller is designed to achieve distributed vehicle control. MCC was originally developed for CAVs; here, we adapt it to mixed-traffic intersections. To ensure consistency, CHVs are guided under the same assumptions as in FTC: cloud-based ROW assignment commands are issued to CHVs, while their decisions are governed by local behavioral models. The communication topology remains PLF.
- **MICS** (Wu et al., 2024a): It extends MCC by adopting a platoon-based framework. A "1 + n" platoon is first formed with a CAV serving as the leader, while CHVs are required to strictly follow their preceding vehicles. Within a platoon, members follow the IDM car-following model. Graph theory is then applied to model conflicts within mixed platoons, and spanning-tree optimization is used to determine the platoon passage sequence. The essential distinction between MICS and MCC lies in the treatment of CAVs and CHVs: MICS groups them into platoons and assigns ROW at the platoon level. In this way, CHVs only follow their immediate leaders through intersections, without engaging directly with conflicting vehicles. Since the original work did not explicitly define communication topologies or vehicle controllers, MICS here adopts MCC's PLF topology and linear feedback controller. Notably, the PLF is refined to the platoon granularity: within a platoon, a leader-follower structure is used, while between platoons, communication occurs between the leaders and the head or tail vehicles of interacting platoons.

4.2. Typical case study

4.2.1. Traffic efficiency and strategy recovery analysis

The ROW assignment scheme provides vehicles with a potential cooperative mechanism. In the MCC scheme, however, the lack of leading vehicles often forces CHVs to yield, creating exposure risks. In this setting, nine CHVs must yield to others when no leading vehicle exists. This exposed state increases the likelihood of CHVs disobeying commands. Once a CHV selfishly occupies the ROW, the MCC scheme is essentially undermined. To prevent such disorder from spreading to all vehicles, the disobedient CHV is removed from the original ROW scheme and temporarily granted the highest ROW priority. In other words, vehicles potentially affected by cascading disruptions must decelerate and yield. These vehicles are primarily those belonging to the ROW layers that the CHV may intrude upon. As shown in Fig. 10, if the target CHV traveling west-east in Layer 10 violates commands and forces its way through, it can at most intrude upon the ROW layers between its predecessor and itself. For example, if the CHV cuts in during the release of Layer 6, its ROW layer moves upward while the ROW of vehicles in Layers 6-9 shifts downward by one layer. This type of strategic-level ROW concession preserves the integrity of the original scheme without re-computation, but at the expense of reduced parallel release capacity within each layer. As illustrated in the MCC trajectory plots, waiting times for cascading vehicles and their queues increase, thereby extending the overall clearance time.

By contrast, MICS provides a conservative yet highly robust solution. It organizes vehicles into platoons to pass through the intersection, fundamentally eliminating the possibility of CHVs infringing upon con-

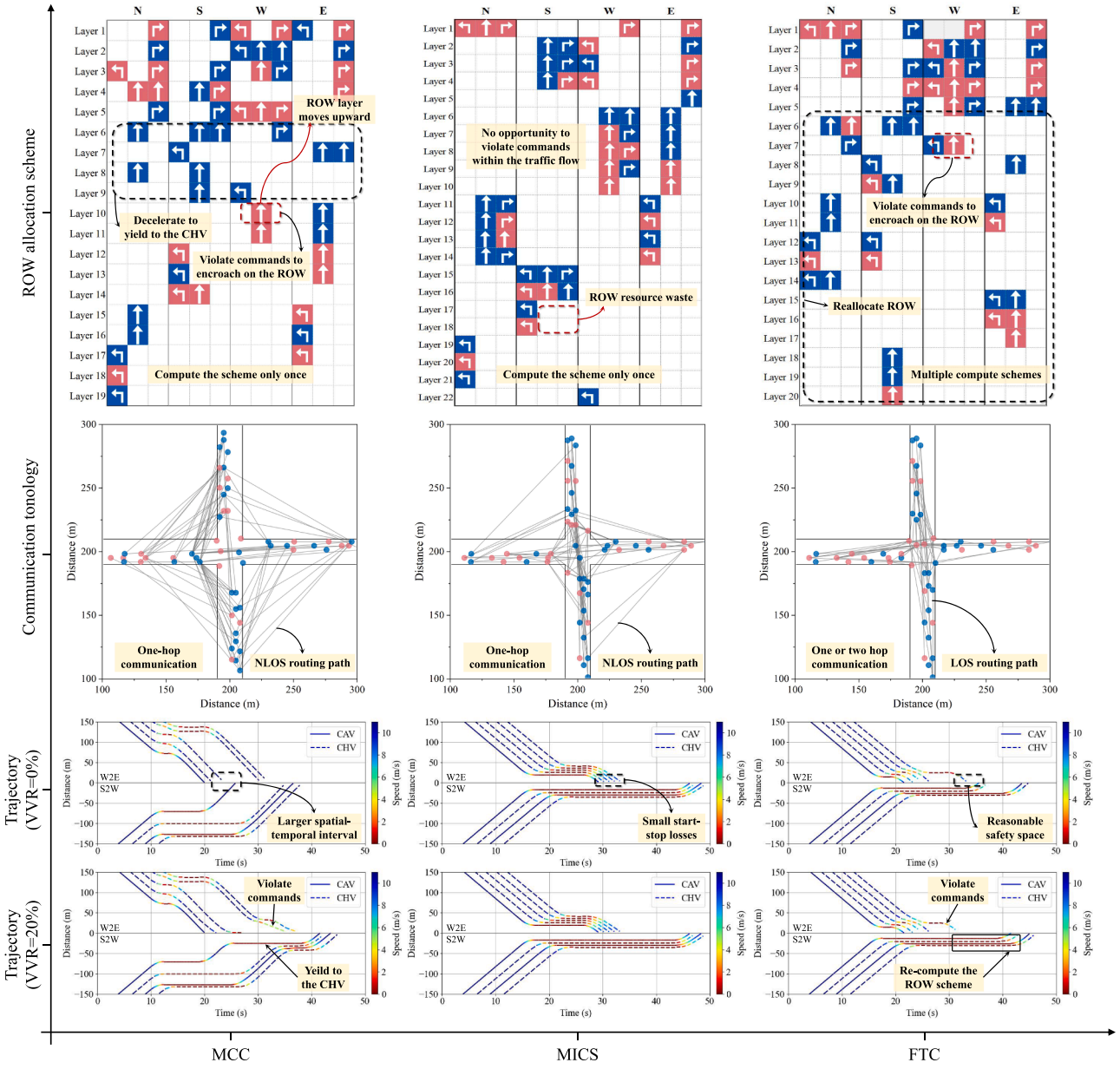

Fig. 10. Experimental results for a vehicle cluster at a typical intersection, illustrating the sequential differences among the methods in ROW allocation schemes, communication topologies, and vehicle trajectories. Blue nodes represent CAVs, while pink nodes represent CHVs. The countermeasures adopted by each method in response to CHV command violations are specifically highlighted.

flicting ROWs. This constitutes a conservative yet safe mechanism, as clearly shown in the MICS trajectory plots. Regardless of a CHV's intention to disobey, the ROW scheme remains intact, highlighting the superior robustness of MICS against strategic interference. However, a key limitation lies in the uneven platoon sizes across approaches, leading to low utilization of certain ROW layers. Thus, MICS eliminates violations entirely but at the cost of larger ROW depth and wasted intersection capacity.

FTC, in comparison, achieves a balance between robustness and efficiency. Only three CHVs face exposure risks, and the number of potentially intruded ROW layers is smaller than in MCC. This advantage arises from reducing CHV exposure risks and minimizing interactions in unavoidable exposure scenarios. Although this preventive arrangement may increase ROW depth, it is mitigated by local trajectory planning, which allows vehicles in the same ROW layer to utilize spatio-temporal resources earlier under safety constraints. Such micro-level adjustments avoid the resource waste caused by MCC's "synchronized release" strategy. Moreover, the re-computation mechanism is critical for FTC to recover from violations. When a CHV violates commands (e.g., a west-east CHV in Layer 7), the re-computation mechanism reallocates ROW for cascading vehicles (Layers 6-20) as a new vehicle cluster. This enables front-row vehicles unable to yield to coordinate ROW allocation with the CHV via local decision-making. As a result, FTC ensures strategic resilience by dynamically adapting ROW, which is validated by trajectory plots showing reduced delays and mitigated cascading effects.

4.2.2. *Communication network and strategy update analysis*

Another key distinction lies in the communication network. While all three methods rely on vehicle-to-vehicle links, their topological properties differ substantially. As shown in Fig. 10, the MCC topology is composed of one-hop edges, many of which are NLOS routing paths blocked by obstacles. Consequently, the network suffers from packet loss and transmission delay. When a disobedient CHV is prioritized for ROW, cascading vehicles (e.g., Layers 6-9) establish one-hop links with the

Table 5
Comparison of traffic efficiency when CHVs follow commands.

Scenario	MPR	Throughput (veh/h)					Average speed (m/s)					Average travel delay (s)				
		MCC	diff.	MICS	diff.	FTC	MCC	diff.	MICS	diff.	FTC	MCC	diff.	MICS	diff.	FTC
1	50%	4355	5.67%	4242	8.49%	4602	3.05	170.16%	2.89	185.12%	8.24	24.72	37.34%	27.91	44.50%	15.49
	70%	4386	6.16%	4471	4.14%	4656	3.11	197.43%	3.73	147.99%	9.25	22.96	54.97%	23.92	56.77%	10.34
	90%	4422	6.92%	4696	0.68%	4728	3.39	192.63%	5.2	90.77%	9.92	21.19	64.94%	18.39	59.60%	7.43
2	50%	4416	24.30%	4770	15.07%	5489	1.73	220.23%	2.66	108.27%	5.54	85.18	70.47%	49.88	49.58%	25.15
	70%	4441	24.90%	4983	11.32%	5547	1.74	358.62%	3.79	110.55%	7.98	81.4	80.87%	46.32	66.39%	15.57
	90%	4472	24.51%	5252	6.02%	5568	1.79	392.74%	4.88	80.74%	8.82	77.33	88.35%	42.01	78.55%	9.01
3	50%	4436	35.35%	5883	2.06%	6004	1.52	40.79%	2.06	3.88%	2.14	143.74	60.51%	60.86	6.74%	56.76
	70%	4494	44.26%	6112	6.07%	6483	1.54	72.73%	2.51	5.98%	2.66	133.75	72.52%	54.41	32.44%	36.76
	90%	4596	48.96%	6365	7.56%	6846	1.55	108.39%	2.77	16.61%	3.23	130.07	79.63%	51.76	48.80%	26.5

CHV to monitor its state in real time. Meanwhile, links between the CHV and its original communication partners (e.g., Layers 9 and 10) are disconnected, as it no longer participates in the original ROW-based strategy.

In MICS, communication is simpler but less resourceful. Its topology also consists of one-hop edges, but with fewer links than MCC, since platoon members only communicate with their immediate predecessors. These links are primarily LOS paths with high communication quality. Nonetheless, head-tail connections between platoons in different approaches still exist, and thus some NLOS links are unavoidable. Given the small total number of links, these few NLOS connections with high delay and low PDR disproportionately degrade overall communication performance. As noted earlier, MICS completely eliminates CHV violations, and therefore the initial communication network remains unchanged throughout the process.

FTC innovates by introducing a dynamic-static coupling network. Nearly all edges bypass occlusions, resulting in LOS routing paths. This improvement stems from the use of two-hop relays within intermediate layers, where vehicles inside the intersection act as relay nodes to forward messages for vehicles with interaction demands from different approaches. This mechanism is essential for alleviating transmission delays and PDR degradation caused by occlusions. When CHVs violate commands, the communication network is updated in tandem with the ROW, thereby ensuring strategic resilience in the communication networking.

4.2.3. Functional synergy of modules

Taken together, the proposed framework integrates multiple layers of coordination, each with complementary functions. The upper level allocates ROW strategically, aiming to minimize CHV violations while maintaining small waiting depths for all vehicles. The middle level generates communication networks aligned with ROW demands, reducing occlusion-related disruptions and ensuring timely and reliable inter-vehicle communication. The lower layer plans and guides trajectories to realize the ROW scheme, efficiently utilizing spatio-temporal resources inside the intersection under safety constraints. Finally, the re-computation module dynamically adjusts ROW schemes after CHV violations, actively adapting to behavioral uncertainties and enabling online updates.

The synergy among modules is critical. While each module fulfills distinct responsibilities, only their coordinated operation leads to overall efficiency improvements. The ROW depth merely reflects the ideal efficiency of vehicle clearance, whereas actual efficiency depends on the accuracy of communication in conveying interaction intentions and vehicle states, combined with the ability of trajectory planning to exploit spatio-temporal opportunities. For instance, although MCC produces the shallowest ROW depth, its requirement for simultaneous release of all vehicles within a layer wastes resources, while frequent CHV violations further undermine efficiency. MICS adopts a similar queue-based design to reduce start-stop losses, yet uneven platoon sizes result in deeper ROW layers. By contrast, FTC, though not yielding the shallowest ROW depth, significantly alleviates cascading disruptions from CHV violations and leverages distributed MPC in a rolling horizon to generate more effective trajectories. Without reliable communication networks, MCC and MICS also prolong clearance times for each layer, as inaccurate information introduces release time gaps at the stop line. Therefore, the three methods differ in unit travel time, which explains the observed variations in traffic efficiency.

4.3. Typical intersection performance analysis

4.3.1. Traffic efficiency

1) Analysis when CHVs follow commands

Experiments are first conducted under ideal conditions (i.e., VVR = 0), where CHVs strictly follow commands. Three performance metrics–throughput, average speed, and average travel delay–are recorded to evaluate the effectiveness of the control strategy. In addition, the differences in FTC compared to MCC and MICS are calculated. The results are presented in Table 5.

FTC outperforms the other two methods across all scenarios. Specifically, the throughput of all methods improves as MPR increases. Compared to MCC, FTC enhances throughput by 5.67% to 48.96%, and compared to MICS, it increases throughput by 0.68% to 15.07%. Notably, MCC experiences a bottleneck as MPR rises, due to its requirement that vehicles with the same priority pass the stop line simultaneously, which wastes some spatial and temporal resources. In contrast, FTC demonstrates superior performance relative to both MCC and MICS, though there is still room for improvement to fully meet traffic demand.

In terms of average speed, FTC maintains good performance, particularly in scenarios with lighter traffic demand. For example, in scenario 1, FTC achieves an average speed of 8.24 m/s to 9.92 m/s, and in scenario 2, 5.54 m/s to 8.82 m/s. As traffic demand increases, the advantage of FTC in this metric diminishes. Nevertheless, the presence of more CAVs consistently improves average speed across all methods.

Similarly, FTC significantly reduces average travel delay. Compared to MCC, FTC improves travel time by 37.34% to 88.35%, and compared to MICS, by 6.74% to 66.39%. This analysis highlights the substantial improvements FTC offers in traffic efficiency when CHVs fully adhere to commands. These advantages remain consistent across varying traffic demands and MPRs, underscoring the robustness of the proposed method.

2) Analysis when CHVs violate commands

The proposed method was also tested under scenarios where CHVs violate the commands. Experimental results were recorded for each of the three metrics mentioned earlier. Notably, the comparison method MICS follows the principle of guaranteeing HDV priority, where HDVs move in platoons by following the leader. This design effectively eliminates the possibility of HDVs violating commands, thus avoiding the trade-off between passage efficiency and strategy robustness. However, whether MICS's design is the most effective strategy for addressing the uncertain behavior of vehicles requires further comparative validation.

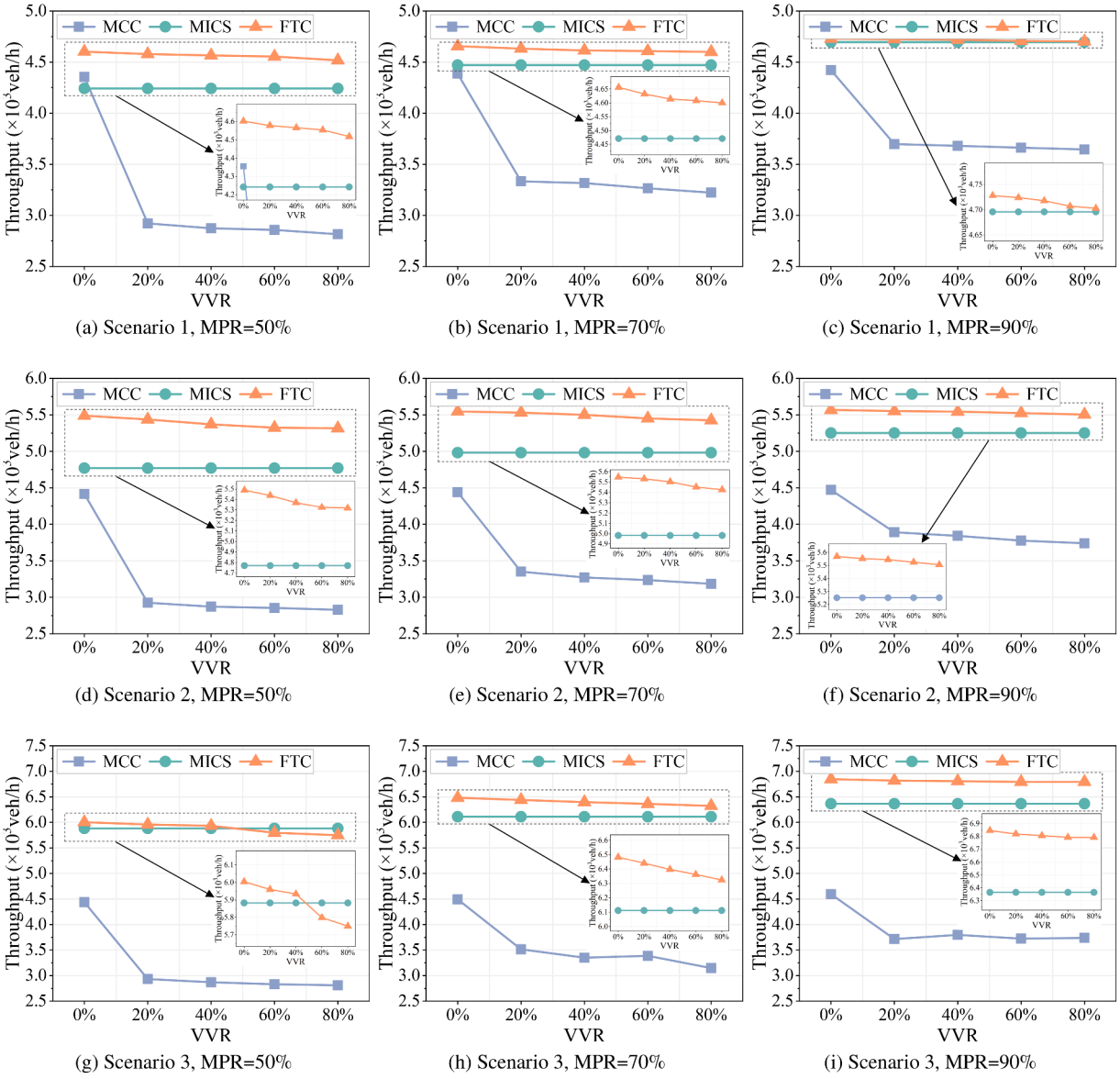

Fig. 11. Comparison of throughput when CHV violates commands.

The throughput results for different VVRs are shown in Fig. 11. Overall, as VVR increases, the throughput of FTC decreases slightly but still maintains a significant advantage over MCC and MICS. This is because CHVs violating commands increase the re-computation workload, reducing the efficiency of the ROW allocation scheme. MCC is more sensitive to VVR, experiencing a substantial throughput decline when VVR reaches 20%, with a decrease of 32.90% to 33.90% at MPR = 50%. Beyond this point, the throughput of MCC decreases more gradually as VVR increases. This is due to MCC's default emergency avoidance strategy for all vehicles, regardless of how many violate commands. The primary difference lies in the additional time CHVs spend passing through the intersection. In contrast, the throughput of MICS remains unaffected by VVR, though its performance still lags behind that of FTC. This reflects that a strict platoon strategy may not necessarily outperform single-vehicle control that incorporates collaboration. Overall, FTC demonstrates a marked improvement in throughput, with a smooth variation in response to changes in VVRs.

To further assess the impact of VVR on vehicle speed, we calculated the Average Speed Reduction Rate (ASRR) for both MCC and FTC, as shown in Fig. 12. The ASRR represents the percentage reduction in average speed for each scenario compared to the baseline at VVR = 0. As illustrated in Fig. 12, the ASRR for MCC exhibits a sharp initial increase, followed by a slower rise, which varies significantly with different traffic demands and MPRs. In contrast, the ASRR for FTC remains relatively stable. Notably, in scenario 3, which involves relatively heavy traffic, the ASRR for FTC ranges from 0.9% to 8.3%, outperforming MCC by a significant margin. Even in scenarios with lower MPRs, FTC consistently outperforms MCC, with reductions in speed ranging from 4.0% to 18.8%, 9.4% to 32.7%, and 0.9% to 6.5%. This improvement in FTC's performance has been supported by Table 5. It highlights FTC's superior average speed at VVR = 0, demonstrating its effectiveness in maintaining both higher average speed and a more favorable overall performance trend under different VVRs.

Additional tests were conducted under different VVRs, in order to further investigate the performance of the proposed method on vehicle travel time. Fig. 13 presents both the individual distributions and statistical results of travel delays. The statistical analysis reveals that, similar to the previous metrics, FTC shows relatively stable average and median travel delays, with small variation. In contrast, MCC's travel delays are more affected by VVR. MICS exhibits travel delays that fall between MCC and FTC, and these delays decrease as MPR increases. This indicates that the conservative platoon-based operation of MICS out-

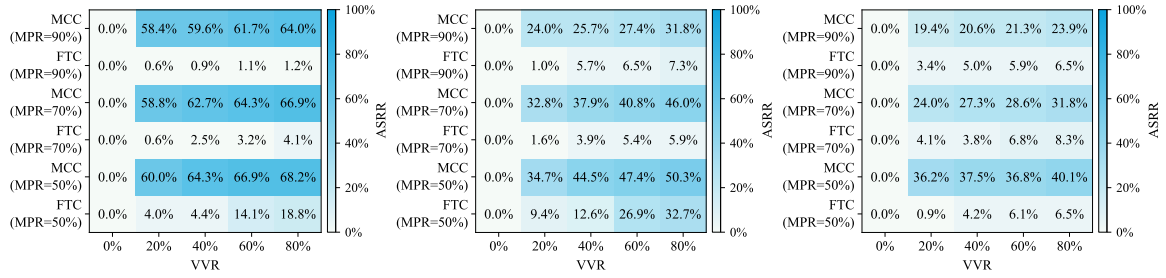

(a) Scenario 1 (b) Scenario 2 (c) Scenario 3

Fig. 12. Comparison of the average speed reduction rate (ASRR) when CHVs violate commands. Since MICS conservatively eliminates the possibility of CHV violations, its passage scheme is unaffected by VVR and therefore not applicable to the ASRR analysis.

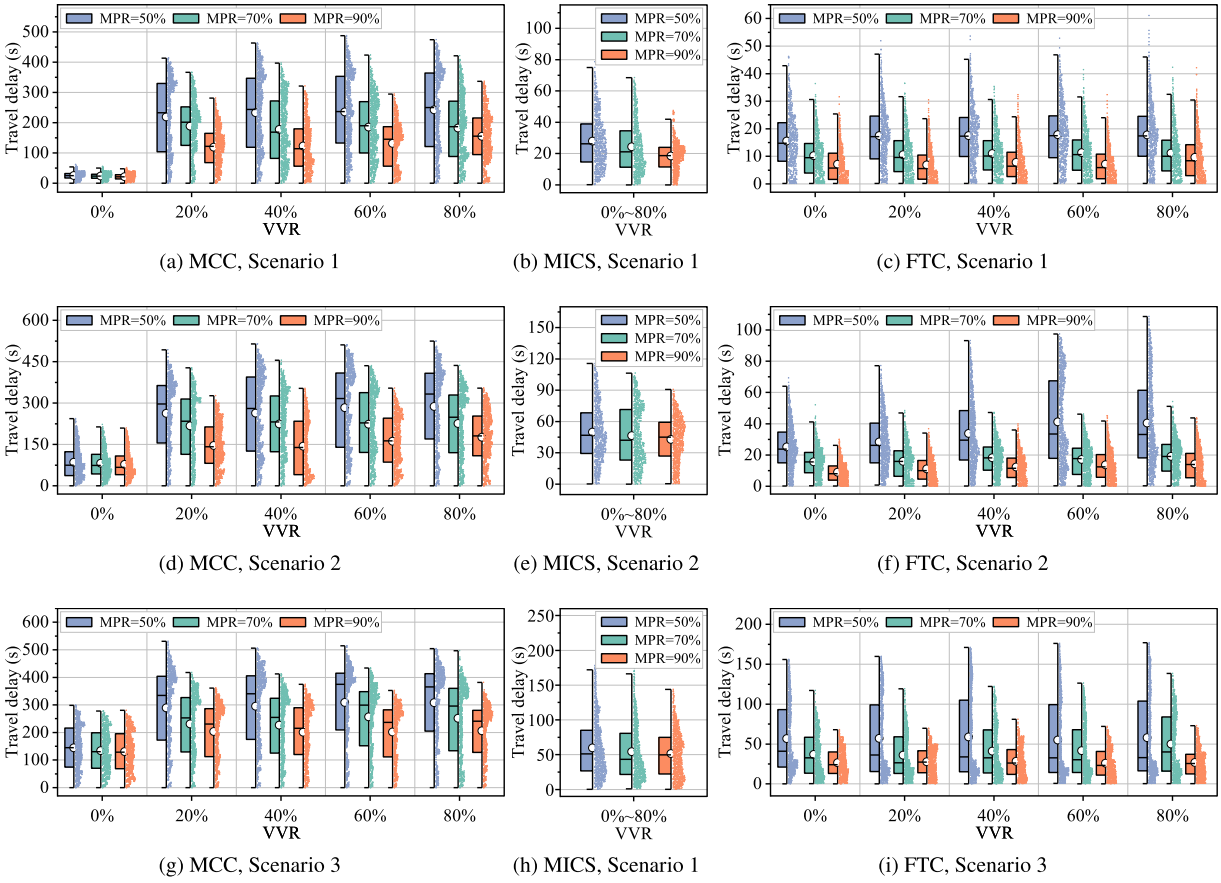

(a) MCC, Scenario 1 (b) MICS, Scenario 1 (c) FTC, Scenario 1

(d) MCC, Scenario 2 (e) MICS, Scenario 2 (f) FTC, Scenario 2

(g) MCC, Scenario 3 (h) MICS, Scenario 1 (i) FTC, Scenario 3

Fig. 13. Comparison of travel delay when CHV violates commands.

performs individual-level ROW allocation in continuous traffic flows, but partial underutilization of ROW resources results in greater overall scheme depth, and thus lower efficiency compared to FTC. Moreover, the interesting insight is that the individual distribution of FTC's travel delays is concentrated in the lower delay intervals, with a long-tailed distribution in the higher intervals. In comparison, MCC's delays are more heavily concentrated in the higher delay range, indicating that most vehicles experience longer waiting times. This analysis, both for individual and statistical results, suggests that FTC effectively enhances intersection efficiency through fault-tolerance mechanisms, especially when dealing with varying numbers of vehicles violating commands.

4.3.2. Communication overhead

To compare the reliability of the communication networks in FTC, MCC, and MICS, the packet delivery rate and average transmission delay were evaluated.

1) Packet delivery rate

The packet delivery rate (PDR) represents the probability of a message packet being successfully received, which is influenced by factors such as distance and occlusion. The simulation results are presented in Fig. 14. The PDR of FTC under various traffic demands ranges from 88.70% to 97.31%, significantly outperforming MCC and MICS, which range from 71.97% to 87.58% and 76.68% to 82.51%, respectively. FTC demonstrates consistent superiority across different VVRs and MPRs. This advantage is attributed to the dynamic-static coupling networking mechanism of FTC, which enables the selection of relay nodes with better LOS conditions for message forwarding. The multi-hop transmission routing paths effectively avoid occlusion caused by buildings and trees along the roadside, mitigating signal shadow fading. In contrast, MCC and MICS exhibit lower PDRs because their transmission routing paths fail to bypass occlusion. Furthermore, it is observed that FTC and MICS are largely insensitive to VVR. Interestingly, CHV command violations

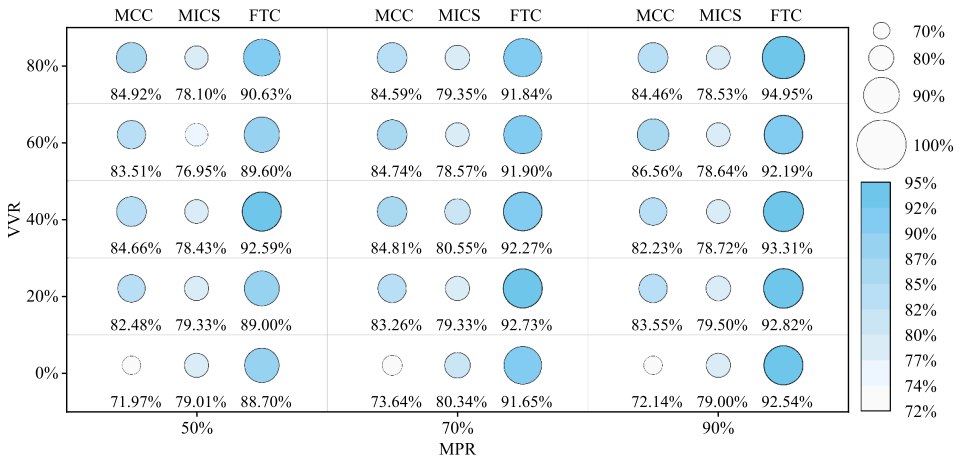

(a) Scenario 1

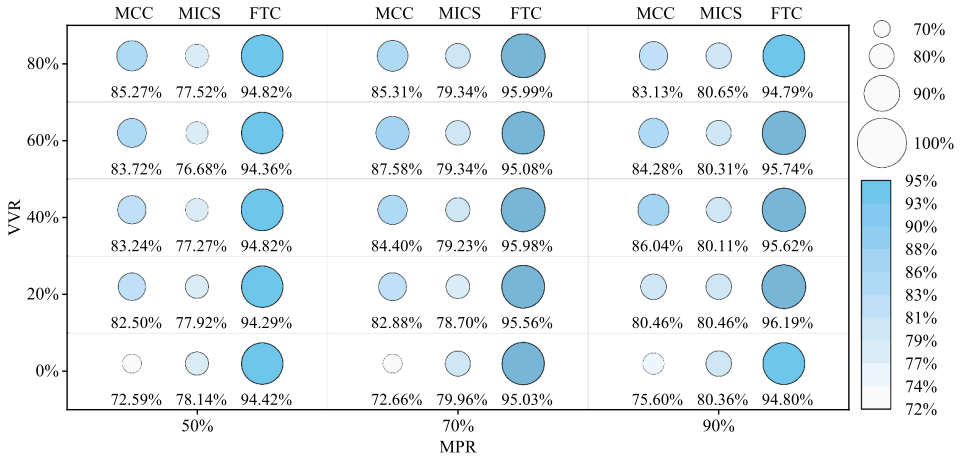

(b) Scenario 2

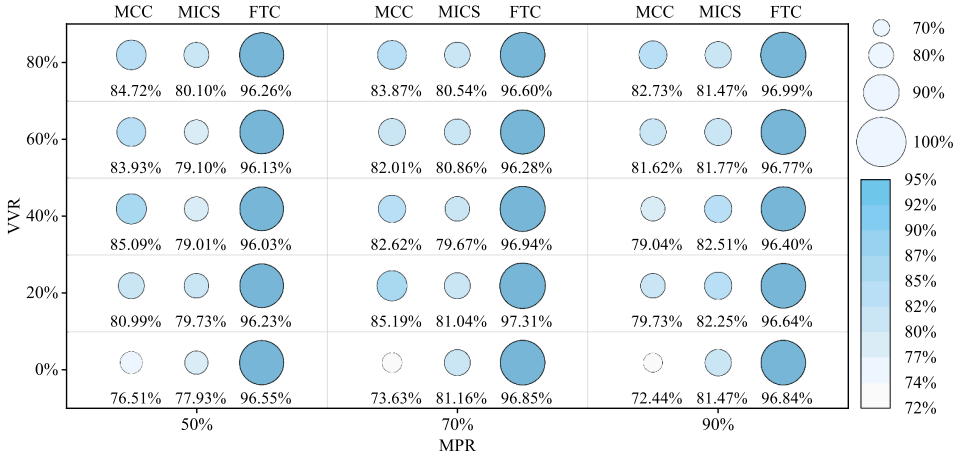

(c) Scenario 3

Fig. 14. Comparison of average packet delivery rate under different methods.

enhance the PDR of MCC. This is because reduced intersection traffic efficiency in such scenarios leads to vehicle congestion near the intersection, shortening communication distances and increasing the prevalence of LOS conditions. Overall, FTC has high robustness in the PDR metric.

2) Average transmission delay

The transmission delay is defined as the time required for a message packet to travel from the sending vehicle to the receiving vehicle via single-hop or multi-hop wireless transmission in the air medium. Table 6 compares the average transmission delay across different methods. It is observed that FTC and MCC exhibit lower transmission delays compared to MICS. This can be attributed to the requirement of MICS for both the leader and trailer of each platoon to communicate, in addition to the internal establishment of a communication topology through the PLF. These processes impose a relatively high communication overhead. When more message packets are transmitted over the

Table 6
Comparison of average transmission delay (ms) under different methods.

Method	VVR	Scenario 1			Scenario 2			Scenario 3		
		MPR = 50%	MPR = 70%	MPR = 90%	MPR = 50%	MPR = 70%	MPR = 90%	MPR = 50%	MPR = 70%	MPR = 90%
MCC	0%	6.42	6.42	5.98	6.01	5.63	5.51	5.13	5.23	5.33
	20%	4.64	4.38	4.54	4.90	4.70	4.72	4.59	4.11	4.66
	40%	4.40	4.31	4.46	4.69	4.44	4.34	4.21	4.48	4.74
	60%	4.43	4.30	4.17	4.55	4.40	4.63	4.33	4.49	4.63
	80%	4.34	4.33	4.91	4.44	4.58	4.53	4.21	4.45	4.43
MICS	0%	37.65	33.62	36.54	38.82	35.09	33.89	35.87	32.01	31.37
	20%	37.00	36.31	36.19	38.85	36.52	34.12	32.23	32.18	31.15
	40%	37.56	34.72	36.53	38.34	35.99	33.70	34.96	35.34	30.71
	60%	38.49	36.77	37.66	38.76	35.53	33.90	35.05	32.25	31.84
	80%	37.80	36.58	37.62	38.38	36.00	34.07	35.27	33.52	32.16
FTC	0%	6.46	4.61	4.38	3.81	4.43	5.23	2.48	2.77	2.74
	20%	5.49	5.64	4.30	4.25	4.00	3.79	3.07	2.46	3.22
	40%	3.98	4.43	3.45	3.76	3.41	3.10	2.99	2.94	3.00
	60%	6.00	5.18	5.66	4.26	4.02	3.08	2.65	2.83	2.83
	80%	4.93	4.66	3.54	3.45	2.98	3.34	2.76	2.71	2.33

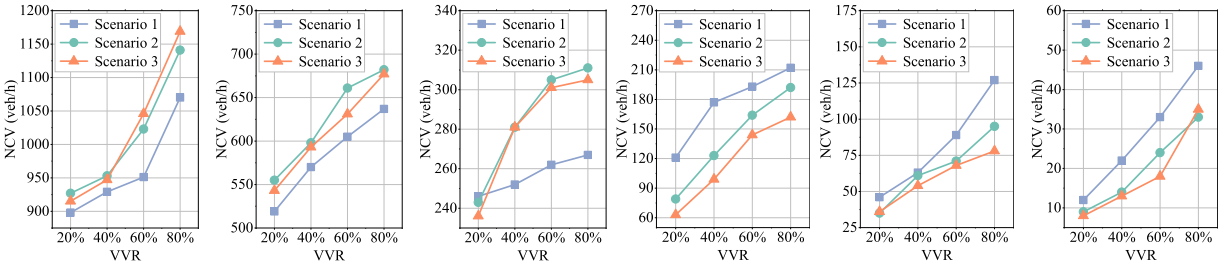

(a) MCC, MPR=50% (b) MCC, MPR=70% (c) MCC, MPR=90% (d) FTC, MPR=50% (e) FTC, MPR=70% (f) FTC, MPR=90%

Fig. 15. Comparison of the number of command violations.

same link, the transmission time increases accordingly. In contrast, FTC and MCC involve fewer interacting vehicles, resulting in a reduced number of effective messages that need to be transmitted, thereby lowering the transmission delay. Additionally, traffic demand significantly impacts FTC's transmission delay. Under current traffic demands, higher vehicle density shortens the communication distance between vehicles. This, combined with an improved PDR, leads to a further reduction in transmission delay for FTC.

4.3.3. Computational cost

This section examines the effectiveness of the proposed method in mitigating the uncertain behavior of CHVs and evaluates the computational cost incurred during method execution and re-computation.

1) Number of command violations

The number of command violations (NCV) quantifies the CHVs' subjective encroachment into the ROW. It serves as an indicator of the method's capacity to handle uncertain behaviors and maintain the resilience of intersection passage strategies. Hourly NCV measurements were conducted across various scenarios, as illustrated in Fig. 15. The FTC demonstrates a significant reduction in NCV compared to MCC across all traffic demands and MPRs. This improvement is attributed to FTC's collaborative mechanism, which minimizes opportunities for CHVs to violate commands. While NCV under FTC increases with higher VVRs, the rise remains minimal relative to the total number of CHVs in the system. Furthermore, heavier traffic demands appear to contribute to a reduction in NCV under FTC. This occurs because larger vehicle clusters expand the search space for collaborative scenarios, enabling the generation of more optimal solutions. Consequently, FTC effectively reduces command violations, particularly at heavily congested intersections, underscoring its robustness in complex traffic environments.

2) Computational time

We evaluate the overhead of the proposed method in terms of total computation time (TCT) and average computation time (ACT). TCT refers to the total computation time required for ROW allocation and communication networking during one hour of intersection operation. ACT represents the average computation time per vehicle cluster. Fig. 16 illustrates the results of these two metrics for the proposed FTC. The TCT of the FTC ranges from 30 s/h to 120 s/h, indicating that the method has low computational complexity and imposes minimal computational cost in practical applications. Similarly, the ACT is acceptable, typically completing ROW allocation for each vehicle cluster in less than 1 s. Notably, the ACT includes the time spent on re-computation, meaning the computation time for each individual ROW allocation and communication networking is even lower. Moreover, both TCT and ACT decrease with increasing MPR, as fewer CHVs reduce the frequency of re-computation. Conversely, an increase in VVR leads to higher values for both metrics for the opposite reason. Additionally, TCT exhibits a performance inversion in Fig. 16c. This is because, under low traffic demand, the size of each vehicle cluster in the control zone is relatively small, resulting in a higher number of clusters per hour. Under high MPR in such scenarios, the gap in ACT between Scenario 1 and Scenario 3 narrows, leading to a corresponding change in TCT.

4.4. Real-world intersection performance analysis

To further evaluate the effectiveness of the proposed framework under realistic intersection conditions, experiments were conducted for both compliant and non-compliant CHV behaviors (with a VVR of 20%), using an MPR of 70% as a representative case. The results for the CG-JN and QL-RM intersections are summarized in Tables 7 and 8, respectively.

Across both intersections, FTC consistently outperformed MCC and MICS in terms of traffic flow efficiency, particularly by reducing average travel delay. These findings highlight the framework's capacity to mitigate low-speed congestion during peak demand. With respect to communication performance, FTC achieved the lowest average PDR and maintained low transmission delay, while also delivering millisecond-

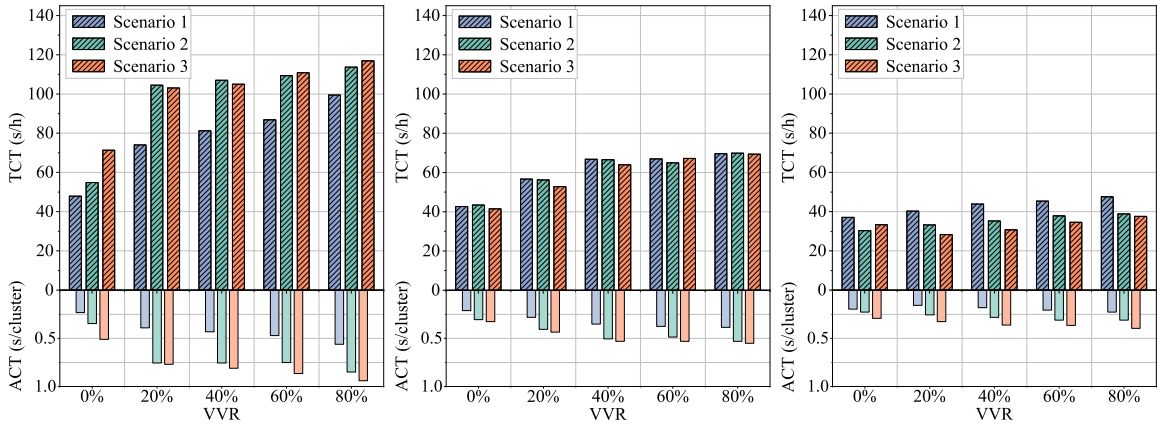

Fig. 16. Comparison of the total computational time and average computational time.

Table 7
Comparison of metrics performance for CG-JN intersection.

Category	Metric	MCC		MICS		FTC	
		VVR = 0%	VVR = 20%	VVR = 0%	VVR = 20%	VVR = 0%	VVR = 20%
Traffic efficiency	Throughput (veh/h)	3875	2606	4702	4702	4733	4712
	Average speed (m/s)	4.08	1.18	4.38	4.38	5.21	4.88
	Average travel delay (s)	93.67	281.21	50.57	50.57	40.01	45.02
Communication overhead	Average packet delivery rate	70.34%	75.45%	78.77%	79.05%	93.56%	94.11%
	Average transmission delay (ms)	5.45	5.18	36.76	36.28	4.86	4.37
Computational cost	Number of command violations (veh/h)	0	537	0	0	0	97
	Average computation time (s/cluster)	0.497	0.492	0.269	0.269	0.462	0.638
	Total computation time (s/h)	32.8	22.14	17.754	17.754	40.67	56.14

Table 8
Comparison of metrics performance for QL-RM intersection.

Category	Metric	MCC		MICS		FTC	
		VVR = 0%	VVR = 20%	VVR = 0%	VVR = 20%	VVR = 0%	VVR = 20%
Traffic efficiency	Throughput (veh/h)	3460	3093	3477	3477	3494	3487
	Average speed (m/s)	6.35	2.79	8.15	8.15	9.74	9.59
	Average travel delay (s)	23.52	65.02	12.65	12.65	7.86	8.07
Communication overhead	Average packet delivery rate	69.84%	80.60%	69.90%	68.23%	89.77%	90.15%
	Average transmission delay (ms)	8.79	7.36	17.14	17.98	7.05	7.21
Computational cost	Number of command violations (veh/h)	0	519	0	0	0	40
	Average computation time (s/cluster)	0.0215	0.0327	0.016	0.016	0.036	0.039
	Total computation time (s/h)	1.72	1.70	1.28	1.28	5.54	6.00

level ACT, which is sufficient to support real-time online applications. Although FTC incurred relatively higher TCT than the other methods, the additional computational cost is justified by the substantial gains in both traffic efficiency and communication reliability.

These advantages were preserved even under conditions where CHVs violated commands. Interestingly, MCC exhibited improved communication metrics in such chaotic scenarios. This counterintuitive result arises because vehicles tended to decelerate and yield to non-compliant CHVs, leading to temporary clustering near the intersection. While such clustering may improve communication conditions, it simultaneously degrades traffic efficiency. Moreover, the reduction in released vehicles lowers the overall TCT, as fewer vehicles are processed centrally for right-of-way allocation.

A comparison between the two intersections further reveals notable insights. As traffic demand increases and conflict relationships become more intricate, the relative advantages of FTC become more pronounced, particularly in enhancing both traffic efficiency and PDR. Furthermore, when transitioning from the QL-RM to the more complex CG-JN intersection, FTC exhibited a much slower growth in TCT compared to the alternatives. Specifically, while MCC increased by 12.02-19.07 times and MICS by 12.86 times, FTC rose by only 6.34-8.36 times. This result underscores the proposed framework's superior computational scalability.

4.5. Sensitivity analysis of cluster size

Fleet size (N_G) is a key determinant of the layer depth in ROW schemes. To examine its influence, a sensitivity analysis was conducted by varying N_G from 30 to 70 vehicles, thereby exploring practical considerations for applying the proposed framework in real-world contexts. Building on the case studies in the previous section (VVR = 0% and 20%, MPR = 70%), experiments were performed at both the CG-JN and QL-RM intersections.

Fig. 17 presents the results for the CG-JN intersection. Traffic efficiency improves markedly as N_G increases, though the rate of improvement diminishes once N_G reaches approximately 60 vehicles. This suggests that while larger fleets enable more effective coordination of passage sequences, marginal benefits taper beyond a certain threshold.

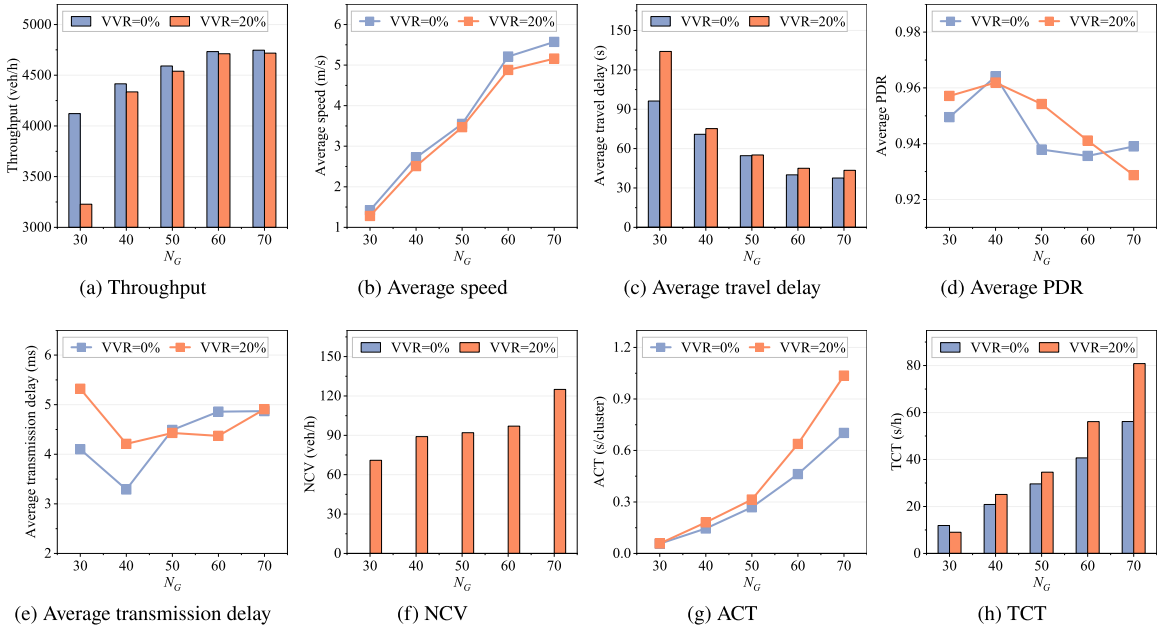

Fig. 17. Comprehensive performance comparison of the CG-JN intersection under different vehicle cluster sizes.

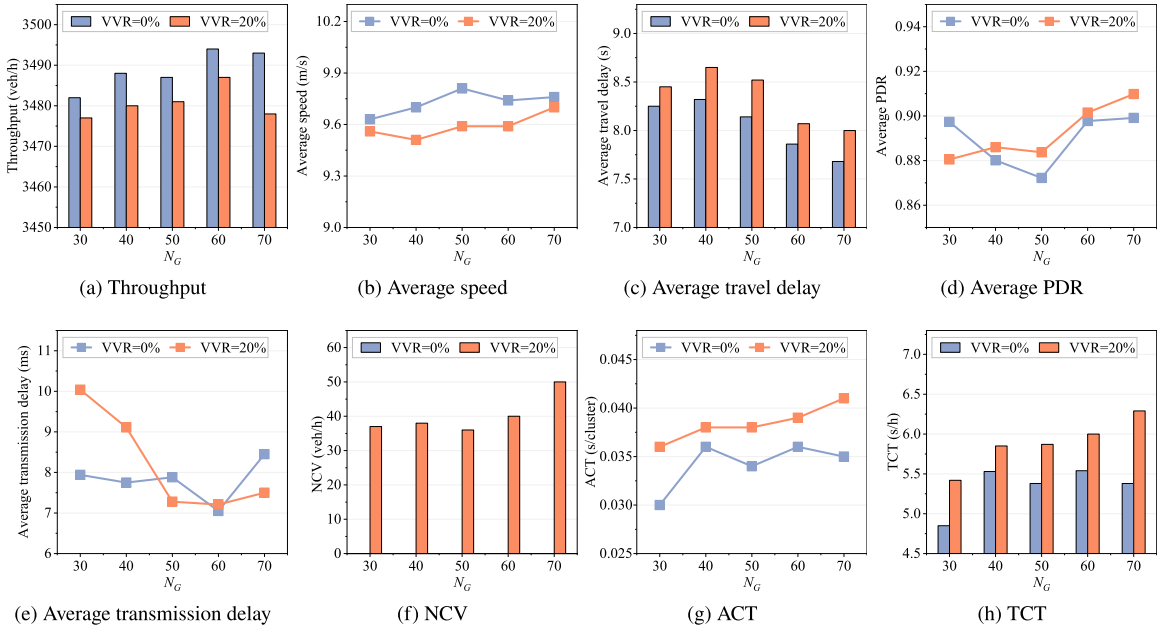

Fig. 18. Comprehensive performance comparison of the QL-RM intersection under different vehicle cluster sizes.

Communication overhead exhibits an initial improvement, followed by a slight rebound before stabilizing. This pattern arises because when N_G is small, controlled vehicles cluster near the intersection, supporting high communication quality. As N_G grows, however, more vehicles queue upstream, enlarging inter-vehicle distances and thereby reducing communication quality to some extent. In terms of computational cost, NCV shows a clear upward trend, indicating more frequent re-computations with larger N_G. Both ACT and TCT follow similar trajectories, as higher vehicle volumes simultaneously increase the scale of individual computations and the frequency of re-computations.

Results for the QL-RM intersection, shown in Fig. 18, reveal broadly consistent patterns. However, the magnitude of fluctuations across performance metrics is smaller than at CG-JN. This difference is mainly attributable to the lower traffic demand at QL-RM: as N_G increases, most vehicles within the study area are already covered, resulting in less pronounced variation.

A cross-intersection comparison indicates that N_G exerts a substantial influence on traffic efficiency, communication overhead, and computational cost. The extent of this influence depends on the intersection layout and traffic demand configuration, yet the underlying trends remain consistent. These findings suggest that in practical engineering applications, the selection of N_G should be tailored to local traffic conditions to balance efficiency, communication performance, and computational feasibility.

5. Conclusions

This paper proposes a fault-tolerant collaboration method with hierarchical control to address traffic management at unsignalized intersections with human-machine mixed driving. An edge-end cooperative computing architecture is designed to construct a cyber-physical system for this scenario, where the MEC and vehicles collaborate hierarchically to achieve cross-system optimization of traffic and communication. To validate the proposed method, several simulation experiments based on SUMO are conducted, considering different vehicle arrival rates and vehicle violation rates. Furthermore, the applicability of the FTC framework was validated through transfer and evaluation at two real-world intersections with distinct layouts and traffic demands. The results demonstrate the effectiveness and resilience of the proposed FTC in various scenarios. It is not only effective in synthetic environments but also scalable and practical in realistic urban settings.

The findings show that FTC significantly reduces the likelihood of uncertain behaviors (i.e., CHVs violating commands) by rationalizing the ROW allocation scheme. While such behavior cannot be fully eliminated, FTC effectively mitigates the degradation of traffic efficiency caused by these uncertainties. The spatio-temporal embedded safety gap model ensures vehicles pass through the intersection without collision, even when uncertain behaviors prevent feasible trajectory planning. Additionally, the motif-based dynamic-static coupling network improves packet delivery rate and reduces transmission delays. The MEC maintains low computational cost during both ROW allocation and networking stages, indicating that the re-computation process does not result in excessive computational burden. Overall, the proposed method performs well in terms of traffic efficiency, communication overhead, and computational cost, confirming its practical feasibility.

Future work will focus on the following areas. First, in this study, the definition of uncertain behavior is restricted to CHVs encroaching upon the ROW by violating assigned commands. We plan to extend this definition to encompass other behaviors, such as CHVs voluntarily yielding their ROW, thereby enhancing the scalability of the proposed method to a broader range of low-frequency, long-tail scenarios. Second, the paper primarily addresses high MPR scenarios for CAVs, but we will explore collaboration mechanisms for low MPR scenarios to cover a broader range of penetration levels. Finally, we aim to strengthen the system's defense capabilities to ensure robust operation in the event of cyber-attacks, an area deserving further exploration.

CRediT authorship contribution statement

Zhigang Wu: Conceptualization, Methodology, Software, Validation, Formal analysis, Writing - original draft, Writing - review & editing, Visualization; **Haipeng Zeng:** Investigation, Writing - original draft, Resources, Project administration; **Di Wen:** Software, Visualization, Writing - review & editing; **Huanting Xu:** Methodology, Writing - review & editing; **Zhaocheng He:** Conceptualization, Resources, Supervision, Funding acquisition, Writing - review & editing.

Data availability

Data will be made available on request.

Declaration of competing interest

The authors declare no competing financial interests in this paper.

Acknowledgement

This research is sponsored by the National Key Research and Development Program of China (2023YFB4301900) and the National Natural Science Foundation of China (U21B2090) and theShenzhen Science and Technology Program (JCYJ20240813151445059). The authors declare no competing financial interests in this paper.

References

Amirgholy, M., & Nourinejad, M. (2024). Connected automated vehicles orchestrating human-driven vehicles: Optimizing traffic speed and density in urban networks. *Transportation Research Part C: Emerging Technologies*, *165*, 104741.

Chen, C., Xu, Q., Cai, M., Wang, J., Wang, J., & Li, K. (2022). Conflict-free cooperation method for connected and automated vehicles at unsignalized intersections: Graph-based modeling and optimality analysis. *IEEE Transactions on Intelligent Transportation Systems*, *23*(11), 21897–21914.

Chen, T., Wang, M., Gong, S., Zhou, Y., & Ran, B. (2021). Connected and automated vehicle distributed control for on-ramp merging scenario: A virtual rotation approach. *Transportation Research Part C: Emerging Technologies*, *133*, 103451.

Chen, X., Zhang, F., Guan, H., & Meng, Q. (2025). Two-dimensional lane configuration design approach for autonomous vehicle dedicated lanes in urban networks. *Transportation Research Part E: Logistics and Transportation Review*, *194*, 103938.

Dubey, S., Cats, O., & Hoogendoorn, S. (2024). Understanding preferences for mobility-on-demand services through a context-aware survey and non-compensatory strategy. *Transportation Research Part C: Emerging Technologies*, *160*, 104455.

Fang, S., Hang, P., Wei, C., Xing, Y., & Sun, J. (2024). Cooperative driving of connected autonomous vehicles in heterogeneous mixed traffic: A game theoretic approach. *IEEE Transactions on Intelligent Vehicles*, (pp. 1–15).

Fang, Y., Min, H., Wu, X., Wang, W., Zhao, X., & Mao, G. (2022). On-ramp merging strategies of connected and automated vehicles considering communication delay. *IEEE Transactions on Intelligent Transportation Systems*, *23*(9), 15298–15312.

Feng, S., Sun, H., Yan, X., Zhu, H., Zou, Z., Shen, S., & Liu, H. X. (2023). Dense reinforcement learning for safety validation of autonomous vehicles. *Nature*, *615*(7953), 620–627.

Garg, M., & Bouroche, M. (2023). Can connected autonomous vehicles improve mixed traffic safety without compromising efficiency in realistic scenarios? *IEEE Transactions on Intelligent Transportation Systems*, *24*(6), 6674–6689.

Greenblatt, J. B., & Saxena, S. (2015). Autonomous taxis could greatly reduce greenhouse-gas emissions of US light-duty vehicles. *Nature Climate Change*, *5*(9), 860–863.

Guo, Q., & Ban, X. J. (2024). Network multiscale urban traffic control with mixed traffic flow. *Transportation Research Part B: Methodological*, *185*, 102963.

Irfan, M. S., Dasgupta, S., & Rahman, M. (2024). Toward transportation digital twin systems for traffic safety and mobility: A review. *IEEE Internet of Things Journal*, *11*(14), 24581–24603.

Jia, S., Zhang, Y., Li, X., Na, X., Wang, Y., Gao, B., Zhu, B., & Yu, R. (2023). Interactive decision-making with switchable game modes for automated vehicles at intersections. *IEEE Transactions on Intelligent Transportation Systems*, *24*(11), 11785–11799.

Jing, D., Yao, E., & Chen, R. (2024). Decentralized human-like control strategy of mixed-flow multi-vehicle interactions at uncontrolled intersections: A game-theoretic approach. *Transportation Research Part C: Emerging Technologies*, *167*, 104835.

Kuroiwa, R., & Beck, J. C. (2024). Parallel beam search algorithms for domain-independent dynamic programming. In *Proceedings of the AAAI conference on artificial intelligence* (pp. 20743–20750). (*vol. 38*).

Li, D., Zhang, J., & Liu, G. (2024a). Autonomous driving decision algorithm for complex multi-vehicle interactions: An efficient approach based on global sorting and local gaming. *IEEE Transactions on Intelligent Transportation Systems*, *25*(7), 6927–6937.

Li, H., Xiao, T., Li, Y., & Feng, Y. (2024b). Development and safety evaluation of an adaptive personalized speed guidance system for on-ramp merging in highway service areas. *Transportation Research Part A: Policy and Practice*, *190*, 104296.

Li, T., Qian, Z., Fan, B., Xu, M., Sun, H., & Chen, Y. (2024c). Integrated optimal planning of multi-type lanes and intersections in a transportation network with mixed HVs and CAVs. *Transportation Research Part E: Logistics and Transportation Review*, *192*, 103814.

Lin, W., & Wei, H. (2023). Cyber-physical models for distributed CAV data intelligence in support of self-organized adaptive traffic signal coordination control. *Expert Systems with Applications*, *224*, 120035.

Lin, Y.-T., Hsu, H., Lin, S.-C., Lin, C.-W., Jiang, I. H.-R., & Liu, C. (2019). Graph-based modeling, scheduling, and verification for intersection management of intelligent vehicles. *ACM Transactions on Embedded Computing Systems (TECS)*, *18*(5s), 1–21.

Liu, C., Jia, H., Huang, Q., & Cui, Y. (2025). A hierarchical intersection system control framework in mixed traffic conditions. *Expert Systems with Applications*, *264*, 125935.

Liu, J., Hang, P., Na, X., Huang, C., & Sun, J. (2024a). Cooperative decision-making for CAVs at unsignalized intersections: A MARL approach with attention and hierarchical game priors. *IEEE Transactions on Intelligent Transportation Systems*, (pp. 1–14).

Liu, J., Qi, X., Hang, P., & Sun, J. (2024b). Enhancing social decision-making of autonomous vehicles: A mixed-strategy game approach with interaction orientation identification. *IEEE Transactions on Vehicular Technology*, *73*(9), 12385–12398.

Liu, J., Zhou, D., Hang, P., Ni, Y., & Sun, J. (2024c). Towards socially responsive autonomous vehicles: A reinforcement learning framework with driving priors and coordination awareness. *IEEE Transactions on Intelligent Vehicles*, *9*(1), 827–838.

Liu, S.-Y., Xiao, J., & Xu, X.-K. (2020). Link prediction in signed social networks: From status theory to motif families. *IEEE Transactions on Network Science and Engineering*, *7*(3), 1724–1735.

Liu, X., Xu, Z., Meng, Y., Wang, W., Xie, J., & Li, Y. (2022a). An elastic-segment-based v2v/v2i cooperative strategy for throughput enhancement. *IEEE Transactions on Vehicular Technology*, *71*(5), 5272–5283.

Liu, Z., Sun, D., Zhao, M., & Zhao, H. (2022b). Cps-based h∞ pinning approach for mixed traffic considering human driver differences. *Transportation Research Part C: Emerging Technologies*, *140*, 103674.

Long, H., Khalatbarisoltani, A., & Hu, X. (2022). Mpc-based eco-platooning for homogeneous connected trucks under different communication topologies. In *2022 IEEE Intelligent vehicles symposium (IV)* (pp. 241–246).

Milo, R., Shen-Orr, S., Itzkovitz, S., Kashtan, N., Chklovskii, D., & Alon, U. (2002). Network motifs: Simple building blocks of complex networks. *Science (New York, N.Y.)*, *298*(5594), 824–827.

Preeti, & Rana, C. (2024). Artificial intelligence based object detection and traffic prediction by autonomous vehicles - a review. *Expert Systems with Applications*, *255*, 124664.

Qin, Z., Ji, A., Sun, Z., Wu, G., Hao, P., & Liao, X. (2024). Game theoretic application to intersection management: A literature review. *IEEE Transactions on Intelligent Vehicles*, (pp. 1–19).

Qiu, T., Zhang, L., Chen, N., Zhang, S., Liu, W., & Wu, D. O. (2022). Born this way: A self-organizing evolution scheme with motif for internet of things robustness. *IEEE/ACM Transactions on Networking*, *30*(6), 2644–2657.

Roy, U., Roy, S., Khan, R., Ghosh, P., & Ghosh, N. (2022). Mcr: A motif centrality-based distributed message routing for disaster area networks. *IEEE Internet of Things Journal*, *9*(24), 25337–25349.

Sheng, Z., Huang, Z., & Chen, S. (2024). Traffic expertise meets residual RL: knowledge-informed model-based residual reinforcement learning for CAV trajectory control. *Communications in Transportation Research*, *4*, 100142.

Shu, K., Mehrizi, R. V., Li, S., Pirani, M., & Khajepour, A. (2023). Human inspired autonomous intersection handling using game theory. *IEEE Transactions on Intelligent Transportation Systems*, *24*(10), 11360–11371.

Song, Y., Liu, Y., Zhang, Y., Li, Z., & Shou, G. (2023). Latency minimization for mobile edge computing enhanced proximity detection in road networks. *IEEE Transactions on Network Science and Engineering*, *10*(2), 966–979.

Sun, S., Cassan, C., & Macharis, C. (2024). Communication is computation: A privacy-protecting routing protocol for physical internet. *Transportation Research Part E: Logistics and Transportation Review*, *191*, 103710.

Świechowski, M., Godlewski, K., Sawicki, B., & Mańdziuk, J. (2023). Monte carlo tree search: A review of recent modifications and applications. *Artificial Intelligence Review*, *56*(3), 2497–2562.

Tam, N. T., Duong, L. H., Binh, H. T. T., & Vinh, L. T. (2024). Subswarm-guided ant colony optimization with enhanced pheromone update mechanism and beam search for VNF placement and routing. *Applied Soft Computing*, *153*, 111263.

Ting, C.-J., & Wu, K.-C. (2017). Optimizing container relocation operations at container yards with beam search. *Transportation Research Part E: Logistics and Transportation Review*, *103*, 17–31.

Wang, D., Li, W., Zhu, L., & Pan, J. (2024a). Learning to control and coordinate mixed traffic through robot vehicles at complex and unsignalized intersections. *The International Journal of Robotics Research*, (p. 02783649241284069).

Wang, S., Li, Z., Wang, B., & Li, M. (2024b). Collision avoidance motion planning for connected and automated vehicle platoon merging and splitting with a hybrid automaton architecture. *IEEE Transactions on Intelligent Transportation Systems*, *25*(2), 1445–1464.

Wang, X., Qin, H., Bian, Y., Zhao, D., & Zheng, N. (2025). String stability under general topologies for CAVs: a coupled sliding surface-based distributed TMPC approach. *Transportation Research Part E: Logistics and Transportation Review*, *194*, 103937.

Wang, Z., An, K., Correia, G., & Ma, W. (2024c). Real-time scheduling and routing of shared autonomous vehicles considering platooning in intermittent segregated lanes and priority at intersections in urban corridors. *Transportation Research Part E: Logistics and Transportation Review*, *186*, 103546.

Wang, Z., Han, K., & Tiwari, P. (2022). Digital twin-assisted cooperative driving at non-signalized intersections. *IEEE Transactions on Intelligent Vehicles*, *7*(2), 198–209.

Wu, R., Jia, H., Huang, Q., Tian, J., Gao, H., & Wang, G. (2024a). Multi-lane unsignalized intersection cooperation strategy considering platoons formation in a mixed connected automated vehicles and connected human-driven vehicles environment. *IEEE Transactions on Intelligent Transportation Systems*, *25*(2), 1569–1585.

Wu, Z., He, Z., Lin, Q., Wang, J., & Li, G. (2024b). Vehicular ad hoc networks topology optimization for autonomous intersection management system: A periodic intervention-based approach. *IEEE Transactions on Intelligent Transportation Systems*, *25*(11), 16005–16023.

Wu, Z., Wang, J., Xu, H., & He, Z. (2024c). T3c: A traffic-communication coupling control approach for autonomous intersection management system. *Transportation Research Part C: Emerging Technologies*, *169*, 104886.

Xie, Y., Kawaguchi, K., Zhao, Y., Zhao, J. X., Kan, M.-Y., He, J., & Xie, M. (2024). Self-evaluation guided beam search for reasoning. *Advances in Neural Information Processing Systems*, *36*.

Xu, B., Li, S. E., Bian, Y., Li, S., Ban, X. J., Wang, J., & Li, K. (2018). Distributed conflict-free cooperation for multiple connected vehicles at unsignalized intersections. *Transportation Research Part C: Emerging Technologies*, *93*, 322–334.

Zhang, M., Fang, Z., Wang, T., Lu, S., Wang, X., & Shi, T. (2025). Ccma: A framework for cascading cooperative multi-agent in autonomous driving merging using large language models. *Expert Systems with Applications*, *282*, 127717.

Zhang, T., Fu, M., & Song, W. (2023). Risk-aware decision-making and planning using prediction-guided strategy tree for the uncontrolled intersections. *IEEE Transactions on Intelligent Transportation Systems*, *24*(10), 10791–10803.

Zhao, X., Gao, Y., Jin, S., Xu, Z., Liu, Z., Fan, W., & Liu, P. (2023). Development of a cyber-physical-system perspective based simulation platform for optimizing connected automated vehicles dedicated lanes. *Expert Systems with Applications*, *213*, 118972.

Zhong, W., Li, K., Shi, J., Yu, J., & Luo, Y. (2024). Reservation-prioritization-based mixed-traffic cooperative control at unsignalized intersections. *IEEE Transactions on Intelligent Vehicles*, *9*(5), 4917–4930.

Zhou, D., Hang, P., & Sun, J. (2024). Reasoning graph-based reinforcement learning to cooperate mixed connected and autonomous traffic at unsignalized intersections. *Transportation Research Part C: Emerging Technologies*, *167*, 104807.

Zhou, D., Ma, Z., Zhao, X., & Sun, J. (2022). Reasoning graph: A situation-aware framework for cooperating unprotected turns under mixed connected and autonomous traffic environments. *Transportation Research Part C: Emerging Technologies*, *143*, 103815.